MIXING TIME STUDY IN AGITATED MULTIPLE-LAMP UV PHOTOREACTOR USING ELECTRICAL RESISTANCE TOMOGRAPHY

By

Zhen Fang Zhao

Bachelor of Petroleum Engineering

University of Petroleum, China, 1999

A thesis

Present to Ryerson University

In partial fulfillment of the

Requirements for the degree of

Master of Applied Science

In the program of

Chemical Engineering

Toronto, Ontario, Canada, 2007

BORROWER'S PAGE

Ryerson University requires the signatures of all persons using or photocopying this thesis. Please sign below, and give address and date.

1.....

2.....

3.....

4.....

5.....

6.....

7.....

8.....

9.....

10.....

11.....

12.....

13. .....

14.....

15.....

Mixing Time Study in Agitated Multiple-lamp UV Photoreactor Using Electrical Resistance Tomography

Zhen Fang Zhao
MASc, Chemical Engineering Program
Ryerson University
Toronto, 2007

ABSTRACT

The present study is devoted to the mixing time investigation in a single stirrer UV photoreactor aiming at the drinking water disinfection process. Electrical resistance tomography (ERT) was employed to measure the mixing quality due to the significant advantages. The reactor was a flat-bottomed cylindrical tank with a diameter of 38.1 cm and a height of 60.1 cm fitted with four symmetrically located vertical baffles. The performances of a 6-blade Rushton turbine and a 4-blade 45° pitched-blade turbine were explored in this study. In the absence of the UV light, four PVC rods were used to replace four UV lamps and evaluate the impact of the locations of the UV tubes on the mixing time. The experimental results demonstrated the feasibility of the ERT system to monitor the mixing process in the UV photoreactor. The ERT results also indicated that the locations of the UV tubes had a significant impact on the mixing performance in such a batch stirred tank reactor. Other parameters encompassing the impeller rotational speed, the impeller type, and off-bottom clearance were presented with respect to the extensive effects on the mixing time and power consumption.

ACKNOWLEDGEMENTS

I would like to express my deep gratitude to my supervisors, Dr. Mehrab Mehrvar and Dr. Farhad Ein-Mozaffari for their attentive and comprehensive guidance, invaluable advice and support throughout the research to accomplish this thesis.

I would like to show my deep appreciation to the faculty members and technologists in Chemical Engineering Department of Ryerson University for the facilities and assistance provided during my program in the university.

I am grateful for financial support of Natural Science and Engineering Research Council of Canada (NSERC) for funding this research.

DEDICATION

A tribute to my father and my mother for the bestowal of a beautiful life to me; for those unconditional love, consistent encouragement and forgiveness throughout my whole life, wherever I am

Dedication also to my special family member in this country —Dou Dou Zhao, for all the unforgettable warmth, love, understanding, patience, and support

TABLE OF CONTENTS

Author's Declaration ii

Borrower's Page iii

Abstract iv

Acknowledgements vi

Dedication vii

Table of Contents viii

List of Tables xi

List of Figures xii

1 INTRODUCTION 1

1.1 Background of UV Disinfection 1

1.2 Research Objectives 2

2 LITERATURE REVIEW 5

2.1 Multiple-Lamp UV Photoreactor 5

2.1.1 Brief Description of Advance Oxidation Processes (AOPs) 5

2.1.2 General Industrial Applications of Photoreactor 8

2.1.3 UV Photoreactor Background Theory 9

2.1.4 Advantages and Disadvantages of Selected Disinfection Processes 14

2.1.5 Established Mixing Characteristic Study of UV Photoreactor 17

2.2 Electrical Resistance Tomography (ERT) System 18

2.2.1 Historical Overview of ERT 19

2.2.2 Application Summarization of ERT in Chemical Engineering 21
2.2.3 Theory of ERT Configuration 22
3 EXPERIMENTAL METHODOLOGY 33
3.1 Experimental Set-Up 33
3.2 Impeller Specifications 43
3.3 Experimental Procedure 47
3.3.1 Mixing Time Study in UV photoreactor 49
3.3.2 Power Consumption in UV Photorector 50
3.4 Experimental Conditions 51
3.5 Measuring System 54
4 RESULTS AND DISCUSSION 63
4.1 Power Consumption Characteristics 63
4.2 ERT Measurements 67
4.3 Mixing Time Studies 69
4.3.1 Effect of locations of UV Tubes 79
4.3.2. Effect of Rotational Speed 97
4.3.3 Effect of Impeller Type 105
4.3.4 Effect of Off-Bottom Clearance 113
5 CONCLUSIONS AND RECOMMENDATIONS 119
5.1 Conclusions 119
5.2 Recommendations 121
NOMENCLATURE 123

REFERENCES 127

APPENDIX: EXPERIMENTAL DATA TABLES 147

LIST OF TABLES

Table 2.1 Table of typical wavelengths (Braun, 1991) 7

Table 2.2 Advantages and disadvantages comparison of chlorination and UV disinfection (Lazarova et al., 1999) 16

Table 3.1 Dimensions of stirred tank UV Photoreactor 39

Table 3.2 Possible locations of UV tubes 43

Table 3.3 Dimensions of impeller RT6 45

Table 3.4 Dimensions of impeller PBTU 46

Table A.1 Dynamic data (impeller RT6, $\mu = 1.002\times10^{-3}$ Pa·s, V = $5.336602\times10^{-2}m^3$) ...147

Table A.2 Dynamic data (impeller PBTU, $\mu = 1.002\times10^{-3}$ Pa·s, V = $5.336602\times10^{-2}m^3$) 148

Table A.3 Dynamic data (impeller RT6, N = 45 rpm, C = 13 cm) 149

Table A.4 Dynamic data (impeller RT6, N = 150 rpm, C = 13 cm) 149

Table A.5 Dynamic data (impeller RT6, N = 250 rpm, C = 13 cm) 150

Table A. 6 Dynamic data (impeller RT6, N = 350 rpm, C = 13 cm) 150

Table A.7 Dynamic data (impeller RT6, N = 500 rpm, C = 13 cm) 151

Table A.8 Dynamic data (impeller PBTU, N = 45 rpm, C = 13 cm) 151

Table A.9 Dynamic data (impeller PBTU, N = 250 rpm, C = 13 cm) 151

Table A.10 Dynamic data (impeller RT6, N = 45 rpm, C = 23.4 cm) 152

Table A.11 Dynamic data (impeller RT6, N = 250 rpm, C = 23.4 cm) 153

Table A.12 Dynamic data (impeller RT6, C =13 cm) 154

Table A.13 Dynamic data (impeller PBTU, C = 13 cm) 155

Table A.14 Dynamic data (impeller RT6, UV tubes location: A) 156

Table A.15 Dynamic data (impeller PBTU, UV tubes location: A) 157

LIST OF FIGURES

Figure 2.1 The spectrum of light (Emperor Aquatics, Inc.) 10

Figure 2. 2 The schematic diagram of electrode arrangement and placement 23

Figure 2.3 Structure of the UMIST Mk.1b data acquisition system (Holden et al., 1998)25

Figure 2. 4 Adjacent electrode-pair sending strategy (Mann et al., 1997; Kaminoyama, 2005; Dickin and Wang, 1996) 28

Figure 3.1 Schematic diagram of the experimental apparatus 34

Figure 3.2 Exterior view of experiment set-up 35

Figure 3.3 Interior view of cylindrical mixing tank with four baffles 37

Figure 3.4 Cover board for mounting UV tubes 40

Figure 3.5 Top view of cover board and UV tubes 41

Figure 3.6 UV tubes location at r = 13 cm, $\theta = 15^{o}$ 44

Figure 3.7 UV tubes location at r = 13 cm, $\theta = 45^{o}$ 44

Figure 3.8 Schematic view of six-blade Rushton Turbine (RT6) 45

Figure 3.9 Schematic view of four blade pitched-blade turbine (PBTU) 46

Figure 3.10 PVC rods employed in UV photoreactor 48

Figure 3.11 Addition point of saline tracer 53

Figure 3.12 ERT system (model: P2000, Industrial Tomography Systems Ltd.) 57

Figure 3.13 ERT sensing system on UV photoreactor 59

Figure 3.14 Sensing system of ERT—dimensions and spacing of four measurement planes 61

Figure 4.1 Experimental power curve for impeller RT6 and PBTU 64

Figure 4.2 Power per unit mass (P_m) versus $N^3D^5\times10^{-4}/V$ for impeller RT and PBTU 68

Figure 4.3 Time series of tomographic images collected from 4 measurement planes following an injection of a high-conductivity tracer for RT6 at r = 10cm, θ = 15°, N = 250 rpm, C = 13cm 73

Figure 4.4 A tomographic image of conductivity distribution measured by plane 3. 75

Figure 4.5 Mixing time at location of UV tubes r = 10 cm, θ = 15° (impeller RT6, N = 250 rpm, C = 13cm,) 77

Figure 4.6 The variation of the mixing time for 18 different locations of UV tubes (impeller RT6, N = 45 rpm, C = 13cm). 81

Figure 4.7 The variation of the mixing time for 18 different locations of UV tubes (impeller RT6, N = 150 rpm, C = 13cm) 83

Figure 4.8 Mixing time versus angle θ (impeller RT6, N = 45 rpm, C = 23.4 cm) 87

Figure 4.9 Mixing time versus radial distance r (impeller RT6, N = 45 rpm, C = 23.4 cm) 88

Figure 4.10 Mixing time versus angle θ (impeller RT6, N = 250 rpm, C = 23.4 cm) 91

Figure 4.11 Mixing time versus radial distance r (impeller RT6, N =250 rpm, C = 23.4 cm) 92

Figure 4.12 Mixing time versus power consumption per unit mass at location A (i.e. r = 16 cm, θ = 45°) 94

Figure 4.13 Mixing time versus power consumption per unit mass at location B (i.e. r = 13 cm, θ = 0°) 95

Figure 4.14 Mixing time versus power consumption per unit mass at location R (r = 11.5 cm, θ = 30°)..... 96

Figure 4.15 Mixing time variation at N = 250 rpm (Impeller RT6, C= 13cm) 99

Figure 4.16 Mixing time variation at N = 350 rpm (Impeller RT6, C = 13cm) 101

Figure 4.17 Mixing time variation at N = 500 rpm (Impeller RT6, C = 13cm) 103

Figure 4.18 Variation of mixing time for 18 different locations of UV tubes (impeller PBTU, N = 45 rpm, C = 13cm)..... 109

Figure 4.19 Variation of mixing time for 18 different locations of UV tubes (impeller PBTU, N = 250 rpm, C = 13cm)..... 111

Figure 4.20 Mixing time versus power consumption per unit mass using different clearances (impeller RT6)..... 114

Figure 4.21 Mixing time versus power consumption per unit mass using different clearances (impeller PBTU)..... 115

CHAPTER 1

INTRODUCTION

1.1 Background of UV Disinfection

In the field of Advanced Oxidation Processes (AOPs), ultraviolet (UV) light disinfection of wastewater and drinking water is rapidly gaining popularity as a viable and beneficial alternative to chlorination. In contrast to chlorine disinfection, UV inactivation is recognized to be cost-effective (Scheible and Bassel, 1981), and forms negligible toxic disinfection byproducts (DBPs) or residuals that would be discharged to the receiving water body (Whitby and Scheible, 2004; Ward and DeGrave, 1978).

In meeting the discharge regulations, nowadays UV disinfection has received wide endorsement as a potent tool in the multiple barrier approach for protection of public health against pathogens and chemical contaminants in wastewater effluents or drinking water. For the latter case, a wide range of research has been triggered to investigate microorganism inactivation by UV light (Wright and Sakamoto, 2001; Snowball and Hornsey, 1988). UV light inactivates microorganisms by damaging their DNA or RNA, thereby preventing pathogen reproduction. It has been proved that nucleotides absorb UV light from 200 to 300 nm, which enables the photochemical reaction that leads to the damage of nucleic acids. Therefore, it is necessary that the electromagnetic spectrum lies between 200 nm and 300 nm for those engineered disinfection UV systems.

The flow behaviour study is of paramount importance in a UV photoreactor. During a photoreaction process, dead zones should be avoided since they result in a low efficiency of the power of lamps, which is the largest component of the UV disinfection implantation and operation costs (Moreira et al., 2007). Thus, a well mixed photoreator is preferred. Furthermore, it has been proved that the intensity of radiation inside the reactor decreases exponentially with the distance from the lamps. In order to assure that each fluid element receives the same radiation dose, choosing the proper circulation rate and the mixing speed will eliminate mass transfer limitations within the reactor, thus enhancing the performance of a UV photoreactor (Tabrizi and Meharvar, 2006).

However, concerning the pollutants degradation or microorganism inactivation by the UV photoreactor, it can be found that the most available literature has been confined to the study of three main aspects within the continuous stirred tank UV photoreactor: (1) hydroxyl radical (·OH) generation mechanisms; (2) the kinetics study and performance evaluation; and (3) the UV photoreactor protocol design. As opposed to this, little effort has been undertaken to describe the mixing characteristics in a batch UV photoreactor, particularly for the mixing time investigation.

1.2 Research Objectives

For the stirred tank reactor, the liquid phase homogenization is of major importance and may be the crucial factor for the success or failure of a process. The liquid is homogeneous when each of its components is perfectly (uniformly) dispersed throughout

the volume of the charge. The efficiency of mixing operations has a big impact on the product quality and production costs (Jahoda and Machon, 1994). The study of the liquid phase homogenization process has often been approached through the study of the 'mixing time' and the 'power input'. Mixing time is the time necessary for attaining the predefined state of homogeneity of the liquid bulk after the addition of a tracer pulse or a second liquid, which is to be homogenized (Giona et al., 2002). It is the main parameter used to define time scale of the macroscopic convective processes in a UV photoreactor. During the disinfection process, mass transfer and therefore, mixing is very important in order to bring the microorganisms to the vicinity of UV lamps and increase the photochemical degradation rate.

Until recently, very little research has been published on the application of electrical tomographic techniques to industrial processes in stirred tank reactors. Several different laboratory and plant-scale experiments were carried out in order to test the performance of the ERT system (Li and Wei, 1999). Because the ERT system can detect local changes in conductivity, this method can be used to study the unsteady mixing dynamics of miscible liquids which have different conductivities. Typically this has been done by injecting a small quantity of strong brine tracer into water and displaying the conductivity field within the tank (Wang and Yin, 2001). After some early studies, Rahimi and Mann (2001) proved that it is possible to capture the details of miscible fluid mixing over a few seconds, and some results were presented with single point addition of a component, using a highly

conducting fluid from a feed reservoir to a different component initially placed in the vessel.

Nevertheless, there is scarce of studies on using ERT system to monitor the homogenization process in connection with the batch stirred tank UV photoreactor. Therefore, the research objectives for the present work are:

- To investigate the feasibility of ERT to monitor the miscible liquid mixing process in the stirred tank UV photoreactor, using a strong brine tracer (NaCl).

- To enhance the understanding of the macroscale mixing in the stirred tank UV photoreactors

- To study the effect of different locations of the UV tubes, impeller type, rotational speed, and clearance on the mixing time

- To determine the power consumption characteristic of two single impellers (i.e. radial and axial impellers), and to compare their performance with respect to the energy efficiency

CHAPTER 2

LITERATURE REVIEW

2.1 Multiple-Lamp UV Photoreactor

2.1.1 Brief Description of Advance Oxidation Processes (AOPs)

A photoreaction is a chemical reaction caused by absorption of radiant energy, which is generally light energy (ultraviolet, visible, or infrared radiation). A photochemical reactor is a reactor where this type of reaction takes place. All of these photochemical processes and related technologies are usually classified as Advanced Oxidation Processes (AOPs) (Glaze et al., 1987) and Advanced Oxidation Technologies (AOTs) or sometimes as Enhanced Oxidation Processes (EOPs).

As a relatively recent vintage, photochemistry is increasingly being used as a powerful wise to eliminate harmful and even toxic emissions into the environment. The most common uses for photoreactors are to break down organic compounds into more desirable constituents that can be present in water or air (Oppenländer, 2003). The reactor can contain a catalyst (such as titanium dioxide, TiO_2) to create free radicals that will attack organic molecules.

For all photochemical reactions, a light source must be applied in the system to induce AOPs. The frequency emitted by the light source, must be the same as the frequency of

absorption of the reactant. In general, four fundamental classes of light source can be considered, including arc lamps, incandescent lamps, fluorescent lamps and tubes, and lasers (Braun, 1991). The typical wavelengths associated with each type of lamp are illustrated in Table 2.1.

To date, there are many photoreactor configurations practically in use to cope with different industrial environment. Based on their geometry and construction, in general, photoreactor can be categorized into various types: cylindrical, immersion, annular, rectangular, parallel plate, etc (Scicchitano, 2003).

For a specific treatment case, the choice of photo-initiated AOPs and photoreactor configuration design depend on various factors: (1) the water or air quality to be treated, (2) the performance related to pollutant removal, (3) the diminution of toxicity, and (4) the possible formation of by-products and the secondary waste. Moreover, capital and operating costs, maintenance and other factors should also be taken into account (Bolton et al., 1998). Also, to choose a desirable UV photoreactor design, the flow behaviour and mass transfer rate in a photoreactor must take into consideration. A number of possible technical solutions may then be found based on these fundamental rules. In the present study, a cylindrical stirred tank UV photoreactor was proposed for drinking water disinfection process in a laboratory scale.

Table 2.1 Table of typical wavelengths for photoreactors (Braun, 1991)

Type of lamp		Wavelength (λ, nm)
Incandescent solids		380.0-1100.0
Mercury vapour arcs	Low pressure	184.9-253.7
	Medium pressure	253.7-579.1
	High pressure	365.0-579.1
Sodium vapour arcs	Low pressure	583.3
	High pressure	400.0-750.0
Xenon arcs		180.0-600.0
Krypton arcs		>750
Fluorescent lamps		380.0-750.0
Actinic fluorescent lamps		300.0-450.0
Lasers		250.0-11000.0

2.1.2 General Industrial Applications of Photoreactor

Numerous industrial applications of the photoreactor have been established and commercialized by the effort of many co-authors in this field. These applications can be mainly summarized into two classes: aqueous system and gaseous systems.

In the past three decades, many researchers have demonstrated the capability of photo-initiated AOPs for the aqueous system, including UV disinfection technology. Critically reviewing and analyzing the most significant industrial and environmental applications, Rice (1997) focused on the O_3, O_3-UV, H_2O_2-UV and O_3-H_2O_2-UV system, and Leitzke et al. (1996) studied the O_3-H_2O_2, H_2O_2-UV, O_3-UV system. Trageser and Greunig (2000) have elaborated the treatment of wastewater from metal processing industries which contain adsorbable organic halogen (AOX), cyanides and organic metal complexes. To reduce persistent organic compounds in nickel containing water, Sörensen and Weckenmann (1988) provided successful practices by using H_2O_2-UV AOPs. Without H_2O_2 addition, another interesting and rare example was referred to as the contact-free batch reactor for AOX diminution from highly contaminated wastewater, which contained halogenated organic disinfectants and aromatic compounds. The reactor was designed with three main components, comprising at least one medium pressure mercury (MP Hg) lamp, a reflector, and a wastewater batch tank. The MP Hg lamp and the reflector were installed within a safety cabinet (so called contact-free) and efficiently cooled by an air ventilation system. It was a special case that resulted from using direct UV radiation solely to achieve effective AOX removal.

On the other hand, AOP technologies are considerably powerful likewise for gaseous systems in industrial and environmental activities. Odour abatement for waste air treatment, air purifier for household or hospital usage, and surface disinfection are of primary interest. As an example, in the recycling industry of household waste (plastics, food cans, containers, etc), sweet-sour substantial odour emissions are produced during industrial activities. Since many odour components absorb UV radiation, a considerable odour reduction can be achieved by direct irradiation of odorous waste air streams with low pressure Hg (HP Hg) lamps at wavelength λ below 300 nm (Oppenländer, 2003). Other published investigations in this field were reported in some scientific literature (Biey and Berstraete, 1999; Dohan and Masschelein, 1987; Ulrich el t al., 2000).

2.1.3 UV Photoreactor Background Theory

Definition of UV Ultraviolet refers to all electromagnetic radiation with wavelengths in the range of 10 to 400 nanometres, or frequencies from 7.5×10^{14} to 3×10^{16} Hz. It is a spectrum of light just below the range visible to the human eye. UV light can be divided into four distinct spectral areas: Vacuum UV (emission wavelength 100 to 200 nm), UV-C (200 to 280 nm), UV-B (280 to 315 nm), and UV-A (315 to 400 nm). Figure 2.1 shows the spectrum of the light (Emperor Aquatics, Inc.).

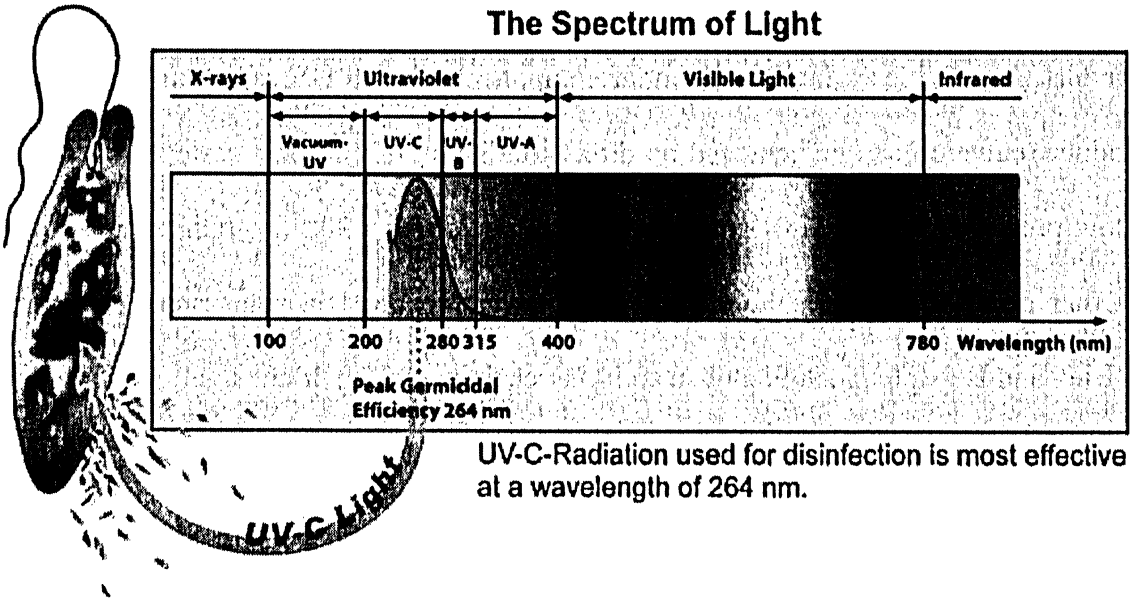

Figure 2.1 The spectrum of light (Emperor Aquatics, Inc.)

Historical Development Ultraviolet radiation has been used for disinfection purposes since the early 20th century. Since then, UV reactors were becoming more important and popular for wastewater (secondary and tertiary sewage effluents) and drinking water disinfection applications. The common definition of the term disinfection usually aims at its medical aspects related to transmissible diseases and to the killing or irreversible inactivation of the disease-causing organisms by use of chemical agents or physical procedures. This includes the destruction of infectious or other undesirable bacteria, pathogenic fungi or viruses and protozoa on surfaces or any inanimate objects (Block, 1993; Harke, 1987). The first application of UV irradiation in drinking water as a disinfection process was performed by Henry et al in 1910. However, general applications were hindered because of high costs, poor equipment reliability, and maintenance problems (Wolfe, 1990; Hoyer, 2004). In Europe, UV has been widely applied for drinking water disinfection since the 1980s, for the control of incidental contamination of vulnerable groundwater and for the reduction of Heterotrophic Plate Counts (Kruithof et al., 1992). The heterotrpphic plate count (HPC), formerly known as the standard plate count is a procedure for estimating the number of live heterotrophic bacteria in water and measuring changes during water treatment.

As a primary disinfection process, another significant contribution to the field of UV disinfection in the US and Europe came after the discovery of the high efficacy of UV irradiation against *Cryptosporidium parvum oocysts* (Clancy et al., 1998) and *Giardia muris*, whereas chemical disinfection with chlorine is not effective against these

pathogenic microorganisms (microbes). In contrast, infectivity of these pathogens is significantly reduced by UV fluences that can readily be applied in drinking water treatment. Disinfection of water employing UV-C radiation has become a convenient and beneficial alternative to the use of chemical processes. UV is now regarded as being broadly effective against all pathogens, bacteria, protozoa and viruses that can be transmitted through drinking water. Hunter (2000) briefly reviewed the developments related to UV disinfection over the past 20 years with references to regulatory and process changes, system design, applicability, and the growth of industry.

Mechanism of UV Disinfection The mechanism of UV disinfection is based on the absorption of UV radiation by proteins, RNA (ribonucleic acid) and DNA (deoxyribonucleic acid) in a given microorganism (von Sonntag, 1987). The absorption of UV radiation by the DNA induces photochemical reaction of DNA components by destruction of sulfur combinations. Thus, the ability of the microorganism to replicate is disrupted, hence the microorganism can no longer infect.

The aim of disinfection techniques is to reduce the number of pathogenic bacteria, viruses, protozoa and spores by inactivation, so that the infectivity of the microorganisms lessens drastically. During a disinfection process, the inactivation of microorganisms follows an exponential decay:

$$\frac{N_t}{N_{t=0}} = e^{-kt} \tag{2.1}$$

Where $N_{t=o}$ denotes the number of microorganisms before treatment, N_t represents the number of microorganisms at time t, K is the rate constant of microorganism inactivation (dimensionless).

With the development of bacteriology, culture media and the gelatine plate, it became possible to obtain the accurate counts of germs by counting the number of colonies developing on these plates under a defined set of conditions. The number of microorganisms is usually stated as colony forming units (CFU) and it is determined by the plate counts (Oppenländer, 2003). Colonies arising from pairs, chains, clusters or single cells are included in the term "colony forming units" (CFU) and all heterotrophic plate count (HPC) are often reported as CFU/mL or CFU/g.

To determine the disinfection efficiency, the reduction factor R_f can be defined as:

$$R_f = \log(\frac{N_t}{N_{t=0}}) \tag{2.2}$$

Where R_f denotes the reduction factor (dimensionless); $N_{t=o}$ denotes the number of microorganisms before treatment; N_t represents the number of microorganisms at time t.

A reduction factor R_f of 4 achieved by a disinfection technique means that the initial number of microorganisms (100%) was reduced by 99.99%.

Two Critical Concepts There are two critical concepts involved in this application: fluence and UV dose. The term fluence (H_o) refers to total amount of energy applied per unit area with SI unit J/m^2. In UV disinfection literature, some authors use UV dose instead of fluence. UV dose was defined for reasons of safeguarding human health in radiology, and it is used in radiation protection.

The idea is based on the product of the reactant concentration (initial or average) with the reaction time or with the quotient of the reactor volume divided by the flowrate in continuous operations (Labas et al., 2006).

$$\text{UV Dose} = I^* \times t_R \text{ in batch systems} \tag{2.3}$$

$$\text{UV Dose} = I^* \times V_R / Q = I^* \times t_M \text{ in continuous flow systems} \tag{2.4}$$

Where I^* means radiation (or light) intensity (Wcm^{-2}), t_R denotes reaction time (s), and t_M has been called the mean residence time (s).

2.1.4 Advantages and Disadvantages of Selected Disinfection Processes

A vast amount of innovative studies have been undertaken for wastewater and drinking water disinfection processes. Besides UV disinfection, several other technologies were

also involved in such a process. For instance, membrane techniques (microfiltration, ultrafiltration, and reverse osmosis) have been employed for water disinfecting potential (Lazarova et al., 1999). However, the most common approach of water disinfection are chlorination by applying molecular Cl_2 (Shang and Blatchley, 2001), hypochlorous acid (HOCl) or chlorine dioxide (ClO_2). Nevertheless, there is a very obvious disadvantage of using this method: the discharge of chlorinated wastewaters may cause acute toxicity to the aquatic ecosystem. This toxicity is due to chlorine and to chlorinated organics produced during chlorination processes. Other viable alternative methods are ozonation, and the use of UV-C radiation (Hoyer, 1996).

Lazarova el al. (1999) provided the comprehensive comparison between chlorination and UV disinfection. It can be summarized in Table 2.2. In addition, Gottschalk et al. (2000) have described the detail analysis concerning ozonation disinfection.

Table 2.2 Advantages and disadvantages comparison of chlorination and UV disinfection (Lazarova el al. 1999)

Chlorination		**UV disinfection**	
Advantages	Disadvantages	Advantages	Disadvantages
Effective pathogen inactivation	Contact time is relatively long (15-30 min)	Very short contact time (in the order of a few seconds)	Fouling of UV tubes must be controlled
Long term effects due to residual Cl_2	Low efficiency towards killing certain parasites (for example, *Giardia muris*)	More effective against a broad range of pathogens in water	Denpending on UV fluence applied, dark repair may lead to a regrowth of some microorganisms
	Poor removal efficiency of inactivation of some viruses, spores, cysts	Protozoan parasites (such as infective *Cryptosporidium parvum oocysts*) can be inactived effectively by radiation with medium pressure Hg lamps (MP Hg) and low pressure Hg (LP Hg) lamps	Large influence of the water quality (such as, total suspended solids, turbidity)
	Formation of toxic disinfection by-products (e.g. chlorite ions ClO_2^-, haloacetic acids $Cl_2CHCOOH$, Cl_3 CCOOH) which are harmful to human health and the environment	Negligible production of toxic by-products; minimal residual effects (if any) that could be harmful to human or environment	Mass transfer limitations
	Investments for safety equipment are necessary for handling Cl_2 and its derivatives	Minimal space requirements to operate; easily automated by UV sensors monitoring, in turn, it is user-friendly, safe, and reliable	
		No chemical added, generated, handled, transported as UV disinfection is a pure physical process	

2.1.5 Established Mixing Characteristic Study of UV Photoreactor

Enormous research dealing with AOPs for environmental applications is well established, especially concerning the UV photoreactor under certain operation conditions. It has been observed that most of the UV photoreactor research has been primarily concentrated on the following areas:

- Hydroxyl radical (·OH) generation mechanism studies for different reacting systems (i.e., O_3, O_3/UV, H_2O_2/UV, O_3/H_2O_2/UV, and TiO_2/UV process, etc) (Legrini et al., 1993; Prousek, 1996; Oppenländer, 2003);

- Kinetics and performance assessing for pollutants degradation or microorganisms inactivation (Yin et al., 2006; Yue and Legrini, 1992; Sundstrom, et al., 1992);

- Designing or selecting specific UV photoreactor protocol for a variety of application cases (Leitner et al., 1997; Dussert, 2005).

However, little studies on the mixing characteristics of UV photoreactors can be found in the open literature although flow behaviour and mass transfer within the system are of paramount importance for the reactor performance. Within this research field, most experiments were conducted on the basis of continuous stirred tank reactors (CSTRs) rather than batch systems. For CSTRs, residence time distribution (RTD) is an important key to the excellent performance of UV photoreactors. RTD is defined as the ratio of

reactor volume and the volumetric flowrate. Some authors have studied RTD using different research approaches (Sahle-Demessie et al., 2003; Demidov et al., 2001; Moreira et al., 2007). Also, several researchers have estimated different aspects on mixing characteristics inside a CSTR UV photoreactor, such as, influence of inlet positions on the flow behaviour using radioactive isotopes as a colour tracer (Moreira et al., 2007) ; characterization of the flow pattern within a vertical flow UV photoreactor by CFD (Computational Fluid Dynamics) numerical modeling (Janex et al., 1998).

Despite a great deal of hydraulic research in the CSTR field, the region of the batch stirred tank UV photoreactor still remains an area that requires further exploration. Little evidence could be found in the literature pertaining to mixing characteristic research in the batch UV photoreactor. Therefore, in this study, ERT was used to study the mixing characteristics of UV photoreactor.

2.2 Electrical Resistance Tomography (ERT) System

To obtain the information on the state and behaviour of the process, a very promising technique named electrical resistance tomography (ERT) was developed which can be adopted in such processes in which the domain is conductive. It is a fast imaging tool and the resistivity distribution inside the object is estimated based on the electrical measurements made on the boundary. It is becoming increasingly popular because of its capacity for providing the potentially detailed information on the complex internal flow,

and multiphase behaviour of the chemical process units (Beck and Williams, 1996; XMa et al., 2006).

2.2.1 Historical Overview of ERT

In recent years, there is a tremendous demand to study the characteristics of the internal contents of process vessels, reactors, separators or pipelines and, more recently, the dynamic behaviour in these systems. For instance, in the oil industry, engineers have been developing designs of non-invasive multicomponent flowmeters to monitor the output of oil wells (Plaskowski et al., 1995). As a relatively new developed imaging technology, tomographic techniques offer this opportunity to quantify the location and the movement of various components in a pipeline or a vessel. Furthermore, this new technology allows chemical process manufacturers to estimate the spatial distribution of phases and chemicals during their processing. This instrumentation provides an exciting basis for the investigations that span a number of scientific disciplines.

The word 'tomography' originates from the Greek words and consists of 'tomos' meaning 'to slice' and 'graph' meaning 'image'. The Oxford English Dictionary defines tomography as "radiography in which an image of a predetermined plane in the body or other objects is obtained by rotating the detector, and the source of radiation in such a way that points outside the plane give a blurred image. Also in the extended use, any analogous techniques using other forms of the radiation are called tomography.

Tomography systems based on electrostatic fields for imaging the conducting (or dielectric) properties of a medium are called electrical tomography systems. Electrical capacitance tomography (ECT), electrical impedance tomography (EIT) and electrical inductance (magnetic) tomography (EMT) produce images based upon the variations in the permittivity, the conductivity and both of these two parameters, respectively. ERT is a particular case of EIT which will also be referred to as EIT. For a process involving mixtures of the ferromagnetic and/or conductive materials, EMT can be selected. Two electrical tomographic techniques have to be combined to give the meaningful measurement results in some certain processes.

The aim of ERT is to reconstruct the conducting (or dielectric) properties of an object from the ERT measurements of electrical signals, taking from all possible views of the sensing electrodes. To obtain the resistance distribution in the domain of interest, the resistance distribution in a cross section can be obtained by injecting the currents (or applying the voltages) on the domain and measure the current (or the voltages) on it via a number of spaced electrodes on its boundary. In this way, ERT electrodes are in contact with the process fluid but do not disturb the process flow pattern. Thus, the technique can be applied to measure the spatial concentration gradients in both the non-intrusive and non-invasive way. It is a simple and inexpensive technique for measuring the distribution of electrical conductivity within multiphase systems and it is typically used for imaging the water/saline, the biological tissues, the geological materials, and the semiconductors.

2.2.2 Application Summarization of ERT in Chemical Engineering

Industrial tomography is often at the forefront transferring the technology from the research laboratory to industrial plants. ERT is rapidly developing due to numerous process applications associated with the conducting fluids. Xie et al. (1995) summarized the characteristics of electrical tomography techniques (ERT, ECT and EMT) and highlighted the applications of ECT and indicated future applications in chemical process engineering. Tapp et al. (2003) reviewed chemical engineering applications of the ECT and EIT, along with various aspects of the design, operation and data processing. Bolton and Primrose (2005) presented recent applications of ERT systems in the pharmaceutical and related application areas.

Based on the discussion above, the applications of ERT in the chemical engineering field can be summarized into five categories, which are: (1) interrogation of mixing processes (Rahimi and Mann, 2001; Li and Wei, 1999; Jia et al. 1995; Wang et al., 2000; Wang and Yin, 2001; Mann, 2005); (2) studying the multiphase flow in pipelines (Lucas et al., 1999; Cory et al., 2000); (3) monitoring the performance of a hydrocyclone (Abdullah et al., 1993; West et al., 2000); (4) investigating a solid-liquid filtration process (Grieve et al., 1999; Yuen et al., 2001; York et al., 2005); (5) applications of ERT in various reactors: measurement and control polymerization (Dyakowski et al. (2000), bubble columns(Toye et al., 2005), fluidized-bed (Hou et al., 2001) and packed-bed reactor (Bolton et al., 2004), etc.

2.2.3 Theory of ERT configuration

A typical ERT system comprises of three main parts: the sensing system, the data acquisition system and the image reconstruction system/host computer. In the following sub-sections, each of these parts will be described in detail.

Sensing System The hardware forming the set of sensors is made up of 16 simple equally spaced rectangular stainless plates, forming into a circular ring. There are 4 such equally axially spaced rings constructed. In some cases, it has been found that 8 or even 1 plane sensing rings can also be adopted. The alternative arrangements of the electrodes can be arranged around a square cross-section as well as a vertical series of electrodes.

Figure 2. 2 shows the sensing electrode array (Dickin and Wang, 1996). Sixteen electrodes are located equidistantly around the vessel wall. Each electrode contacts the inner conductive fluid on the front surface but does not invade the flow.

The electrodes are connected to the data acquisition system by the co-axial cable for reducing the extraneous environmental noise and the interference. A spare electrode is required for grounding purposes to ensure all the voltage measurements are fixed against a common ground source. It is in contact with the internal fluid but positioned away from the measurement electrodes.

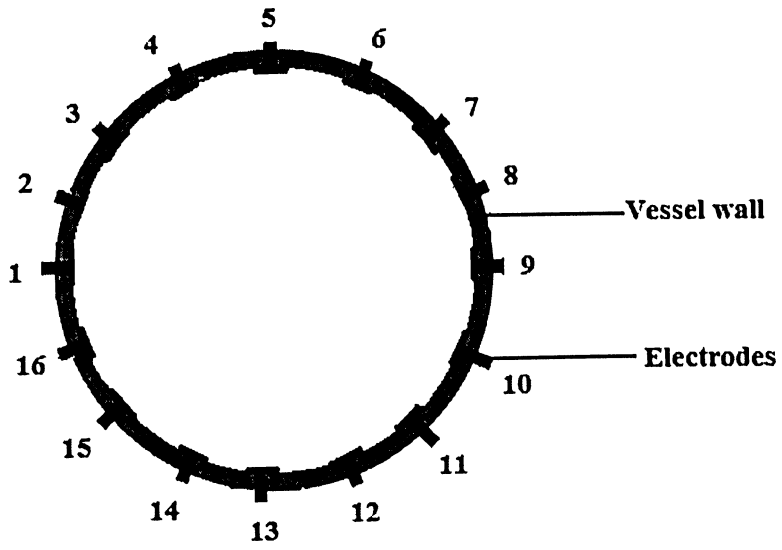

Figure 2. 2 The schematic diagram of electrode arrangement and placement (Dickin and Wang, 1996)

Data Acquisition System An accurate and stable Data Acquisition System (DAS) is a basic necessity for the ERT system. It is responsible for obtaining the quantitative data revealing the state of the conductivity distribution inside the tank or pipelines. This has to be done accurately and quickly in order to monitor the small changes of conductivity in real-time (Williams and Beck, 1995).

Figure 2.3 shows a schematic diagram of the upgraded acquisition system from UMIST Mk.1b (Holden et al., 1998), which is made up of five functional parts. It incorporated signal sources, an electrode multiplex array, voltmeters, signal demodulators, and a system controller.

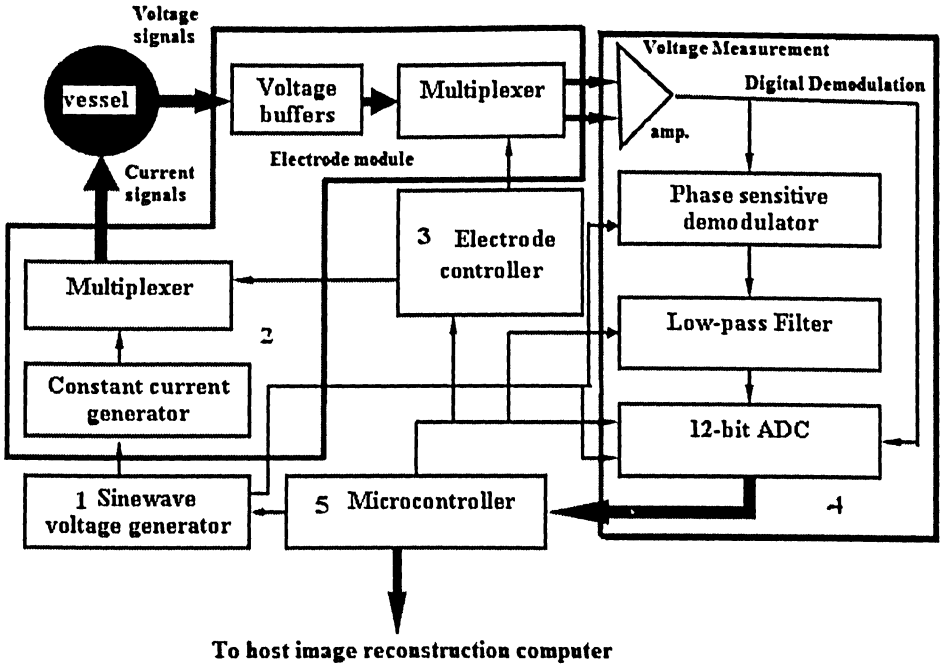

Figure 2.3 Structure of the UMIST Mk.1b data acquisition system (Holden et al., 1998)

In this block diagram, the sine-wave voltage generator was employed to produce a harmonically pure sine-shaped waveform. Initially, monolithic function generators were used to generate the sine wave but were soon replaced by dedicated digital forms in the form of EPROM-based 'staircase' function generators. Multiplexers were necessary in order to 'share' the current source and the voltage measurement stages between any numbers of electrodes. Depending on the strategy used to inject, the current there will be a wide dynamic range of voltages varying from millivolts to volts which the voltage measurement stage must be able to accommodate. Therefore, the instrumentation amplifier was used to solve this problem and it had the ability to reject common-mode signals such as the electrical noise. To optimize their signal-to-noise ratio (SNR), the amplitude attenuation and the phase shift of the injected sine wave signal as a result of passing through a resistive medium were recovered by synchronous digital demodulation techniques. Depending upon a number of criteria, the analogue-to-digital converter (ADC) should be low-cost, fast conversion, high resolution, an in-built sample-and-hold circuit and a bipolar input. Such complexity was very necessary because of: (1) the large number of electrode channel operations (a minimum of 832 for the 8-plane 16-elctrode ring-sensor system); (2) the large stray capacitance of coaxial cable (of which more than 300 m is needed for the associated cabling); (3)and high common voltages (V) with a small responses of the dynamic change (normally of the order μV); and (4) low amplitude of the measurement at the boundary (mV).

The measurement strategy or protocol for probing the conductivity distribution within the vessel via boundary electrodes to obtain the maximum amount of information is of extraordinary importance. Adjacent, opposite, diagonal, and conducting boundary are four main strategies. Some other strategies, such as the linear, the channel and the dual probe measurement strategies have been also employed for different process applications. The measurement protocol for present study was the adjacent strategy.

The adjacent strategy is the commonly used strategy for sensors with insulating boundaries. This measurement protocol is based on injecting current using a pair of neighbouring electrodes and measuring the voltage differences, using all other pairs of neighbouring electrodes, as shown in Figure 2.4 (Mann et al., 1997; Kaminoyama, 2005; Dickin and Wang, 1996). This process is then repeated by injecting current using all other possible pairs of neighbouring electrodes until all the independent measurements have been made. A 16-sensor gives 104 independent measurements. This procedure is executed by the data-acquisition system run by the PC.

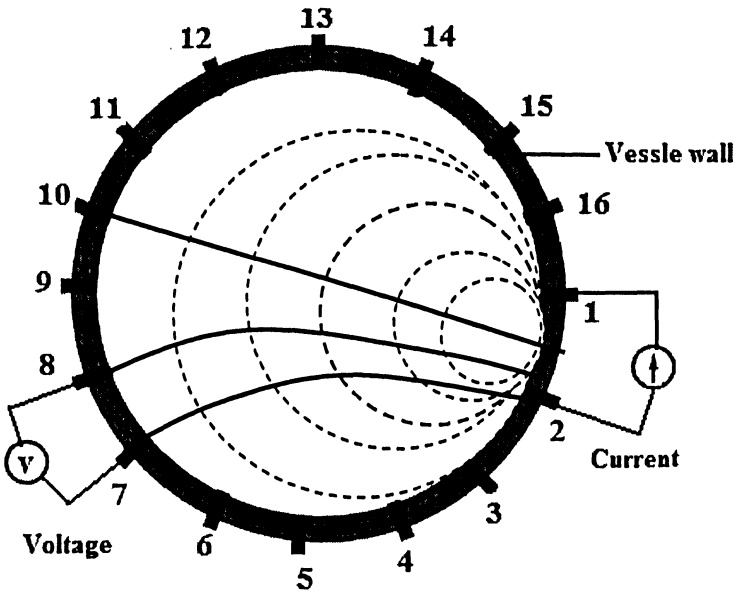

Figure 2.4 Adjacent electrode-pair sending strategy (Equipotential lines, solid; current streamlines, dotted.) (Mann et al., 1997; Kaminoyama, 2005; Dickin and Wang, 1996)

Because of the non-uniform current distribution and the relatively low current density at the centre of the vessel, this strategy is very sensitive to measurement error and noise. However, the strategy requires minimal hardware to implement and reconstruct the image.

Imaging Reconstruction An image reconstruction algorithm is used to determine the internal distribution of the resistance within the process vessel from the measurements acquired from an array of the electrodes mounted on its periphery. The algorithm resides in the host computer connected to the data acquisition system, and can be used both on and off-line. Two algorithms called "qualitative algorithm" and "quantitative algorithm" have been developed, and the images reconstructed by these algorithms are often referred to as "dynamic" and "static", respectively. The more popular algorithm is qualitative algorithm as the images depict the relative change in resistivity against an initially acquired set of reference data, which are usually acquired prior to the start of the experiment under quiescent conditions. On the other hand, "quantitative algorithm" produces an image depicting the values of the resistivity or the conductivity for each pixel.

An imaging reconstruction method named linear back–projection (LBP) was used for the present study. This method (mostly non-iterative) utilizing a sensitivity coefficient weighting method was first defined by Geselowitz (1971) and enhanced by Kotre (1989) for the qualitative algorithm. This is why it is named back-projection method: the potential difference on the surface, i.e. from the adjacent electrodes, is back-projected to

a resistivity value in the area between two equipotential lines. Initially the region between the equipotential lines is assumed to have the homogeneous resistivity, and the potential differences at the electrodes are calculated using the finite element or other suitable techniques. This algorithm can be performed in a single step using a precalculated pixel sensitivity matrix stored in the computer's memory. To reconstruct the image, a matrix/vector multiplication operation is performed on modern computers equipped with floating-point units (Holden et al., 1998). Thus:

$$[P(\sigma_m)]_M = \sigma_0 / (([K]_{M,N}) \cdot [\eta]_N) \tag{2.5}$$

Where σ_m denotes conductivity relative value; P represents column matrix of conductivity relative value at pixel *m;* $[\eta]_N$ means relative value of boundary measurements; M is the number of pixels; N is the number of boundary measurements; $[K]_{M,N}$ is called the normalized sensitivity matrix; and σ_0 is the conductivity for a homogeneous case for the reference measurement.

Using the sensitivity coefficients adopted from the Kotre's (1989) method, the following equation gives the entry of the normalized sensitivity matrix $[K]_{M,N}$:

$$K_{m,n} = \frac{S_{m,n}}{\sum_{n-1}^{N} S_{m,n}} \tag{2.6}$$

Where $S_{m,n}$ denotes sensitivity coefficient and $K_{m,n}$ is the entry of the normalized sensitivity matrix. All parameters in equation 2.5 and 2.6 are dimensionless.

Linear methods are quick, as images are generated by simply multiplying the measurements by a single, pre-calculated matrix. The matrix is the transpose of an estimated solution to the forward problem, based upon either field gradients or more commonly, 'sensitivity maps'. The main advantage of this algorithm is that it can be performed in a single step using a precalculated pixel sensitivity matrix that is stored in the computer's memory. It needs low computation cost and has immunity to the sensor noise. The image is simply reconstructed by a matrix /vector multiplication operation that can be performed rapidly on modern computers equipped with floating-point units. However, the accuracy of the imaging data from the 2-D presumption is limited due to both the 3-D distribution of real electric fields and the LBP algorithm. UMIST developed a "full" 3-D electrical resistance tomographic analysis by Pinheiro et al (1997). More complete details of the preceding qualitative reconstruction method can be found in the literature (Mann et al., 1996).

In the past few years, a number of interesting reconstruction algorithms has been developed and some of them are accepted as being theoretically correct. Another popular algorithm is non-linear Newton-Raphson reconstruction algorithm. For example, Yorkey et al. (1986) used the Newton-Raphson iterative minimization algorithm to solve the inverse problem. It offers more flexibility in the measurement protocol that can be used.

Normally, algorithms based on iterative approaches are often computationally more time consuming, and currently too slow for the real-time image reconstruction.

CHAPTER 3

EXPERIMENTAL METHODOLOGY

3.1 Experimental Set-Up

The experimental setup to study the mixing characteristics of the UV photoreactor is shown in Figure 3.1. The exterior view of the experiment set-up is depicted in Figure 3.2. The stirred tank employed in the present study was a cylindrical flat-bottomed tank (diameter T = 38.4 cm, height H_l = 60.1cm) with four symmetrically located vertical baffles (baffle width B = 3.8 cm) attached to the wall. Figure 3.3 shows the interior view of the cylindrical mixing tank with four baffles. The system was designed with a single impeller, i.e. either a six-blade Rushton turbine or a four blade 45° pitched-blade turbine. The dimensions of the stirred tank UV photoreactor are summarized in Table 3.1.

Four PVC rods (diameter = 2.5 cm) were mounted to the vessel from the top by a specially designed cover board and acted as 4 UV lamps to evaluate effects of the locations of the UV tubes for the mixing time.

Figure 3.4 shows a photo of the cover board. This board allowed UV tubes to slide and change positions in both different angles, and radial distance to the shaft, as shown in Figure 3.5.

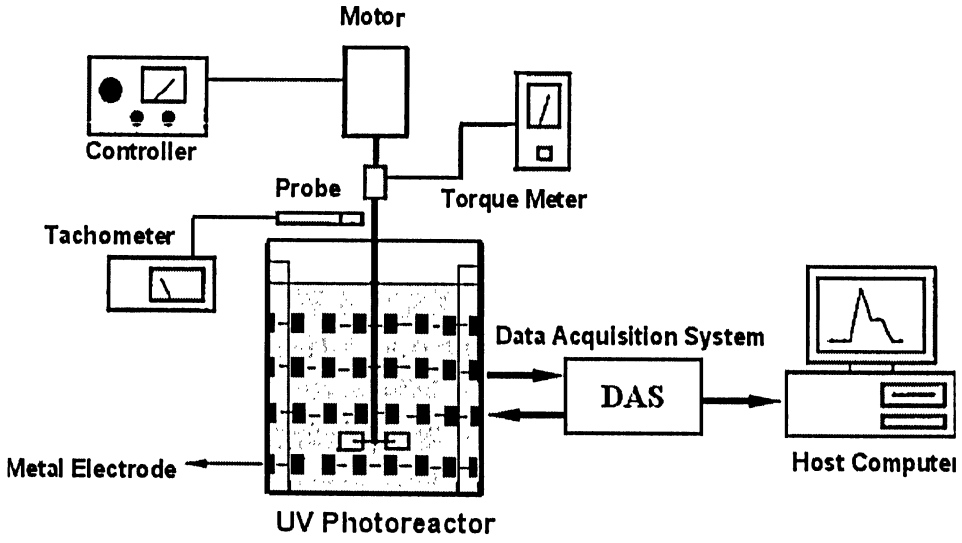

Figure 3.1 Schematic diagram of the experimental apparatus

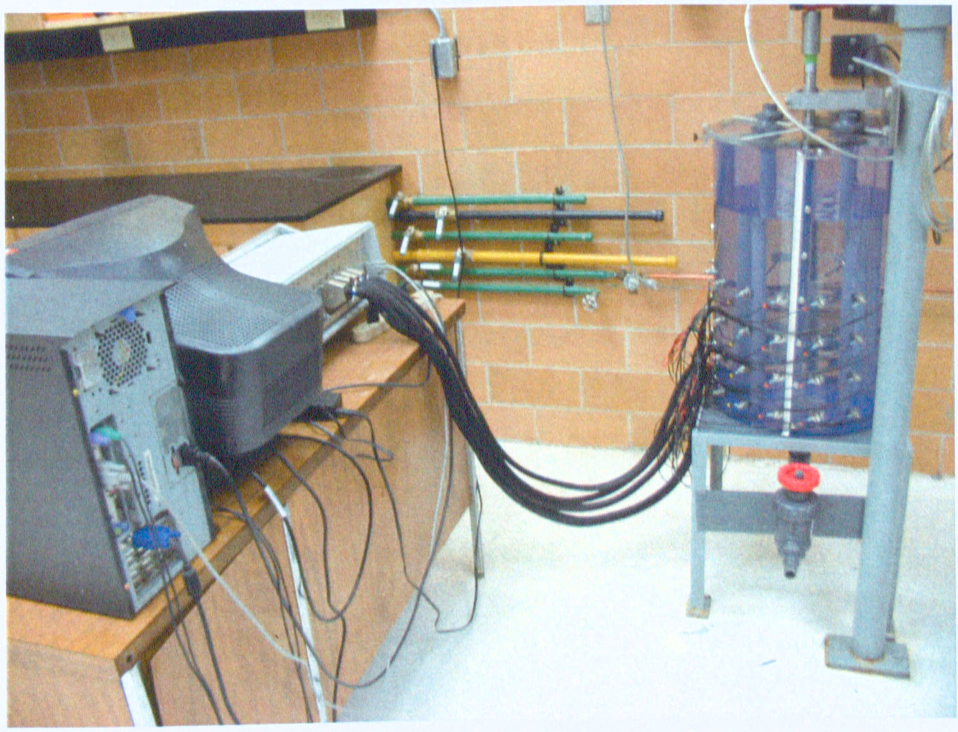

Figure 3.2 Exterior view of experiment set-up

Figure 3.3 Interior view of cylindrical mixing tank with four baffles

Table 3.1 Dimensions of stirred tank UV photoreactor

Tank inner diameter, T (cm)	Tank outer diameter, T_1 (cm)	Tank height, H_1 (cm)	Baffles width, B (cm)	Baffles length, L (cm)	Shaft diameter (cm)	Fluid height, H (cm)
38.4	40	60.1	3.8	58.8	2.5	46.1 (1.2 T)

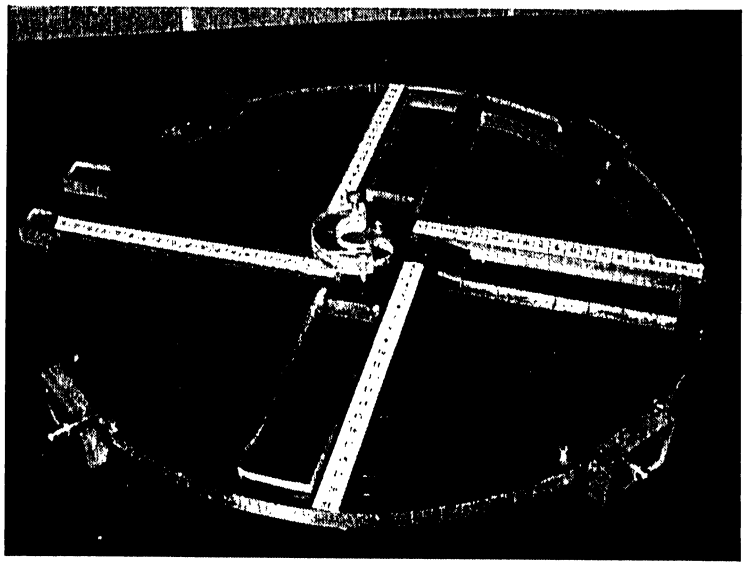

Figure 3.4 Cover board for mounting UV tubes

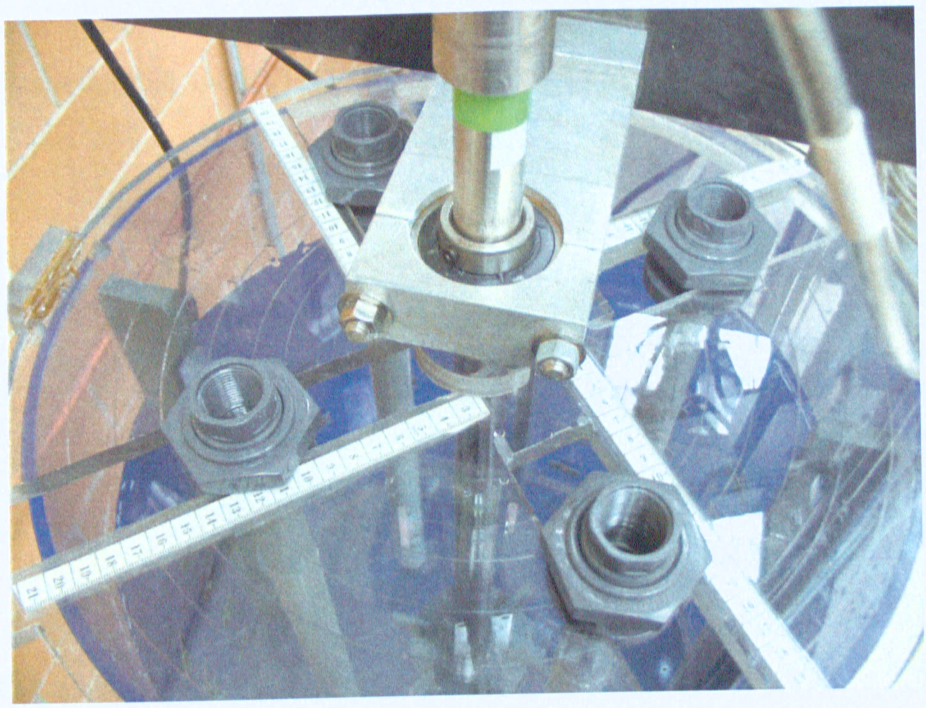

Figure 3.5 Top view of cover board and PVC rods

The locations of UV tubes were specified using θ and r, as shown in Figure 3.6 and Figure 3.7. Accordingly, in total, 18 different locations of the UV tubes were chosen for each impeller rotational speed (as presented in Table 3.2).

Table 3.2 Different locations of UV tubes

The angle θ (deg)	The distance between the UV tube center to the shaft center **r** (cm)				
0	10	11.5	13	-	-
15	10	11.5	13	14.5	16
30	10	11.5	13	14.5	16
45	10	11.5	13	14.5	16

3.2 Impeller Specifications

The stirring action was provided with a standard six-blade Rushton turbine (denoted as RT6) and a 45° 4-blade pitched-blade turbine (denoted as PBTU). Both of these two impellers had the same diameter D = T/3 with the blade height b = D/5. Figure 3.8 and Figure 3.9 show the schematic view of RT6 and PBTU, respectively. The dimensions of both impellers are summarized in Table 3.3 and Table 3.4.

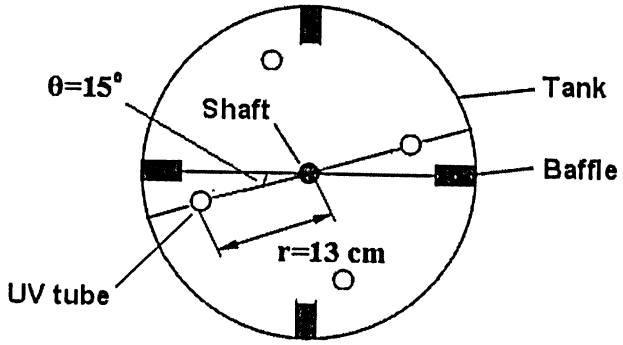

Figure 3.6 UV tubes location at r = 13 cm, θ = 15°

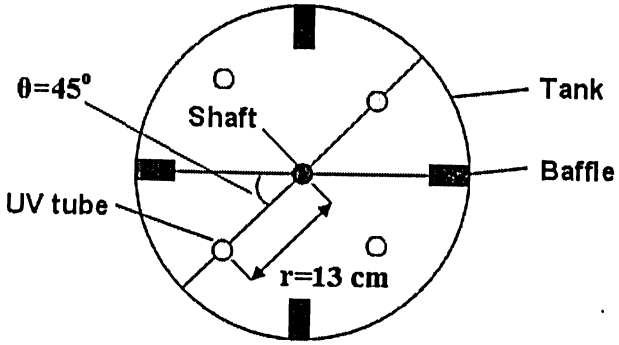

Figure 3.7 UV tubes location at r = 13 cm, θ = 45°

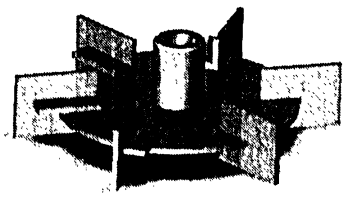

Figure 3.8 Schematic view of six-blade Rushton Turbine (RT6)

Table 3.3 Dimensions of impeller RT6

Impeller diameter, D (cm)	Impeller blade width, a (cm)	Impeller blade height, b (cm)	Impeller disk thickness, h (cm)	Impeller blade thickness, h_1 (cm)
T/3 = 13	D/4 = 3.2	D/5 = 2.6	0.02D = 0.6	0.6

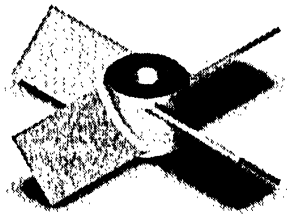

Figure 3.9 Schematic view of four blade pitched-blade turbine (PBTU)

Table 3.4 Dimensions of impeller PBTU

Impeller diameter, D (cm)	Impeller blade width, a (cm)	Impeller blade height, b (cm)	Impeller disk thickness, h (cm)	Impeller blade thickness, h_1 (cm)	Discharge angle, β (deg)
T/3 = 13	D/4 = 3.2	D/5 = 2.6	0.02D = 0.6	0.6	45

3.3 Experimental Procedure

The cylindrical vessel was filled with the experimental liquid (tap water) to a height of 46.1cm. The volume of the UV photoreactor and experimental liquid were 6.94×10^{-2} m^3 and 5.34×10^{-2} m^3, respectively. The motor was then started, which rotated the impeller shaft. A digital tachometer was used to measure the speed of rotation. The power consumed by the impeller was measured using a torque meter (model: 0170/01 MS20RAU, Staiger Mohilo, Germany). The mixing time measurements were carried out by the addition of the saline tracer (NaCl), and subsequently, the time evolution of the tracer concentration was monitored. By applying the ERT system, the conductivity versus time data for each test was acquired and saved on the personal computer (PC), which can then be analyzed for calculating the mixing time. When all of the four planes showed a constant conductivity value, the data acquisition was stopped. The motor was shut down and the liquid was drained. For the next experiment, the vessel was then refilled with fresh tap water.

It should be noted that the experiments were performed by using PVC rods instead of the UV lamps to evaluate different parameter effects on the mixing time, since the PVC rods (diameter 2.6 cm, length 60 cm) used in the experiments had the same external geometry (cylindrical) as UV lamps.

Figure 3.10 shows a photo of the PVC rods that employed in the experiments.

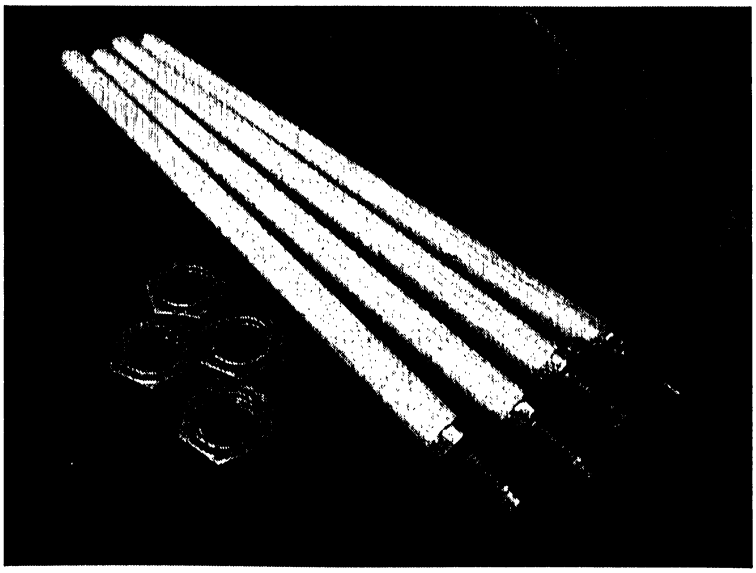

Figure 3.10 PVC rods employed in UV photoreactor

3.3.1 Mixing Time study in UV Photoreactor

The mixing process is usually characterized in terms of the mixing time. The mixing time is the time necessary for attaining a homogeneous state since the time of the tracer injection to a stirred tank reactor. The first thorough analysis of mixing time was reported by Holmes et al. (1964) and Voncken et al. (1964). The approach followed by these authors has become a standard way of describing the tracer dispersion experiments for subsequent research.

An expression for the dimensionless concentration is used to describe a homogeneous mixture (Landau and Prochazka, 1961):

$$c^*(t) = \frac{c(t) - c(0)}{c(\infty) - c(0)} \tag{3.1}$$

Where $c(0)$ represents the initial tracer concentration at time $t = 0$; $c(t)$ is the tracer concentration at time t; and $c(\infty)$ is the final tracer concentration. The unit of the concentration is kgm^{-3}. It is very clear from the above equation that the mixing time t can be defined as the time when $c^*(t) = 1 \pm 0.05$. That is, t is taken as the time at which the concentration of the detecting position reached 95% of the final concentration (completely mixed). The symbol t_{95} has been used in the open literature to represent the mixing time. Compared to other definitions, 95% homogeneity appears to be more appropriate and robust (Ranade et al., 1991; Hiby, 1981).

3.3.2 Power Consumption in UV photorector

The power dissipated by the agitation system is fundamental to any mixing process since energy is needed to homogenize the vessel content (immiscible phases, suspend solids, etc.), and to produce the desired mixing effect. The power consumption is not only a function of the type and the number of the impeller, the fluid properties, and the stirring speed, but also of the geometry of the system, including the impeller spacing and the length of the baffles in the mixing vessel. The power consumed by the individual impeller is usually the major contributing part of the total power consumption of the system, which mainly comprises of the friction, bearing losses, electrical losses, etc.

The total power input of the agitated system can be given by:

$$P = 2\pi N\tau = \omega\tau \tag{3.2}$$

Where P denotes power input (watt); N is rotational speed (rps); τ represents torque (m·N); and ω is called angular speed (radians/s).

Many previous studies have been published regarding power consumption for a single stirrer system. Agitation systems with a single disk turbine (RT) have been studied extensively (Hudcova et al., 1989). In the literature, a flat bladed disk turbine (or disc turbine) if often referred to as Rushton turbine (RT) or the disk turbine (DT). Many investigators have experimentally determined the power characteristics of single impellers (Rushton et al., 1950 a,b; Bates et al., 1963, 1966; Gray et al., 1982; Shiue and

Wong, 1984; Chudacek, 1985). It has been found that the impeller power number, N_p, reaches a constant value for a given geometry if the agitation intensity is high enough to produce the turbulent flow (Re > 10000).

Impeller power number N_p can be determined from the power P (W) required to drive the impeller (diameter D with the unit m) at the rotational speed N (s^{-1}). According to the definition, N_p was calculated from the following equation (Rushton et al., 1950a, 1950b):

$$N_p = P/\rho N^3 D^5 \qquad (3.3)$$

Where ρ is the liquid density (kg/m^3).

In spite of the popular use of dual or multiple impeller systems in chemical industries, only incomplete information in the open literature is available for the power consumption in these systems. Bates et al. (1963) determined the power consumption of the dual pitched-bladè turbine (PBT). Nienow and Lilly (1979) found that the Np for a single RT was 4.9 while that for the two impeller systems was 10.2. Some other studies are available for various configurations in stirred systems (Hudcova et al., 1989; Smith et al., 1987; Lu and Yao, 1991).

3.4 Experimental Conditions

The experiments were carried out at an ambient temperature of 22°C. The working fluid was tap water (ρ = 1000 kg/m^3; μ = 1.00 mPa·s). The total height of the liquid in the

vessel was 1.2 T = 46.1 cm. The tracer liquid chosen was sodium chloride NaCl solution (concentration c = 100kg/m^3) with the injection volume of 50 mL for each test. The tracer injection was performed by a single syringe. The injection point was located midway between the vessel wall and impeller shaft (as shown in Figure 3.11). The vertical location was about below the experimental liquid surface 10 cm.

For each impeller, the mixing time was investigated at five different speeds of rotation. The range of rotational speed in the experiments was from 45, 150, 250, 350 to 500 rpm. Due to this range of speed, the study was limited to the batch mixing of Newtonian liquids (i.e. water) in the fully turbulent regime. Four different clearances (13, 21.45, 29.9 and 38.35 cm) were chosen for both impellers to test the response of the mixing time.

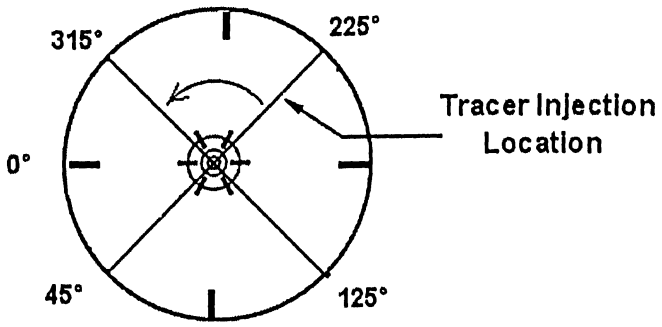

Figure 3.11 Addition point of saline tracer

3.5 Measuring System

Since the first studies of the mixing time in stirred systems in the 1950s (O'Connell and Mack, 1950; Rushton et al., 1950a, b), various methods for estimating the mixing time have been set up based on the experimental analysis of tracer dispersion (Metzner and Taylor, 1960; Biggs, 1963; Rice et al., 1964). During the experiments, the concentration of the tracer was measured at one or several points within the vessel. The classical approach to obtain the response curve from a dispersion experiment was based on the conductivity probes (Shiue and Wong, 1984). More methods were developed based on decolourizations methods (Moo-Young et al., 1972) and on laser-induced fluorescence (Gaskey et al., 1990).

However, each of these methods has some limitations for its application in practice. Although the conductivity probe method is widely used for measuring the mixing time for low viscosity systems, it has been shown that the mixing time also depends on the size of the conductivity probe (Rielly and Britter, 1985), thus making the measurements results inaccurate.

Compared to the measurements techniques above, in contrast, ERT was adopted in the present study due to its significant advantages. It provides a unique wise to interpret the complexities of the objects structure that are often very difficult to understand using other sensing techniques. As a promising imaging technique that emerged in the 1990s, it is capable of meeting many significant requirements: safety, cost, and speed.

As shown in Figure 3.12, the ERT system applied in this experimental work consisted of three main parts: the sensing system, the data-acquisition system and the image reconstruction system (model: P2000, Industrial Tomography Systems Ltd.). Four-plane assembly of sensing rings, each containing 16 metal electrodes were constructed for the ERT sensing system. The electrodes were made of stainless steel and the dimensions of each electrode were: length 30mm, width 20mm, and thickness 1mm.

To monitor the mixing process inside the stirred vessel, the data-acquisition system and the image reconstruction system were also used to get the internal distribution of the conductivity within the process vessel.

For the sensing system, Figure 3.13 shows a photo of the ERT sensing system. The dimensions and the spacing of the four planes, numbered from the top downward, are indicated in Figure 3.14.

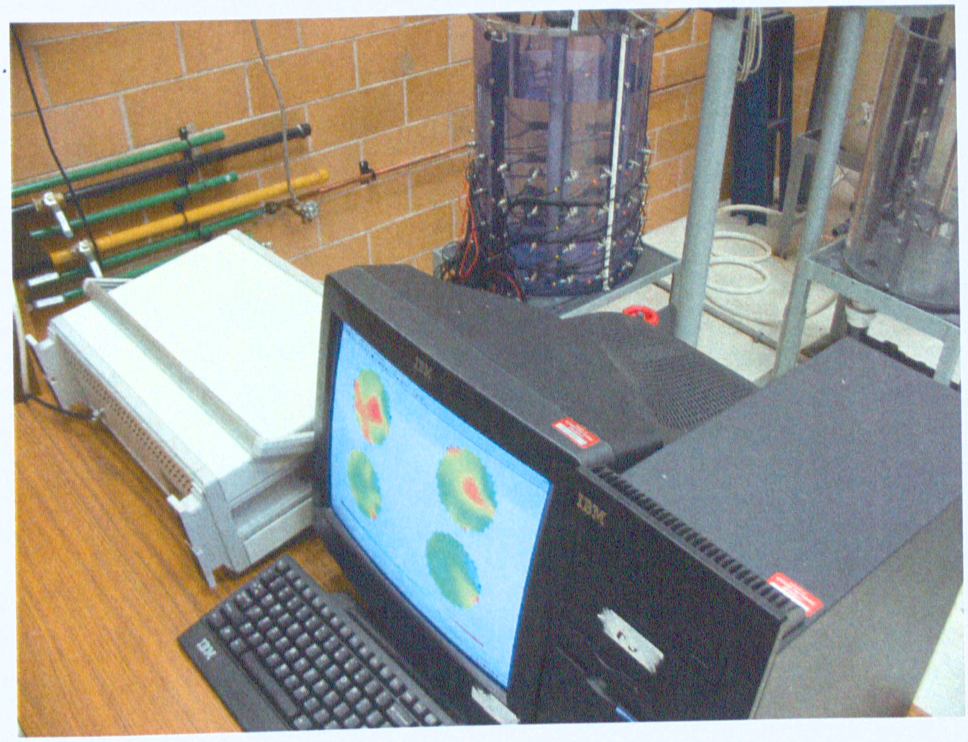

Figure 3.12 ERT system (model: P2000, Industrial Tomography Systems Ltd.)

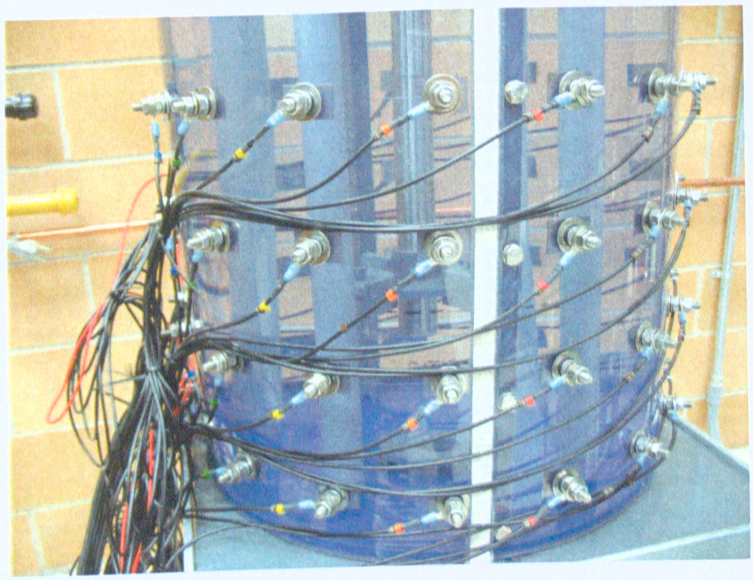

Figure 3.13 ERT sensing system on UV photoreactor

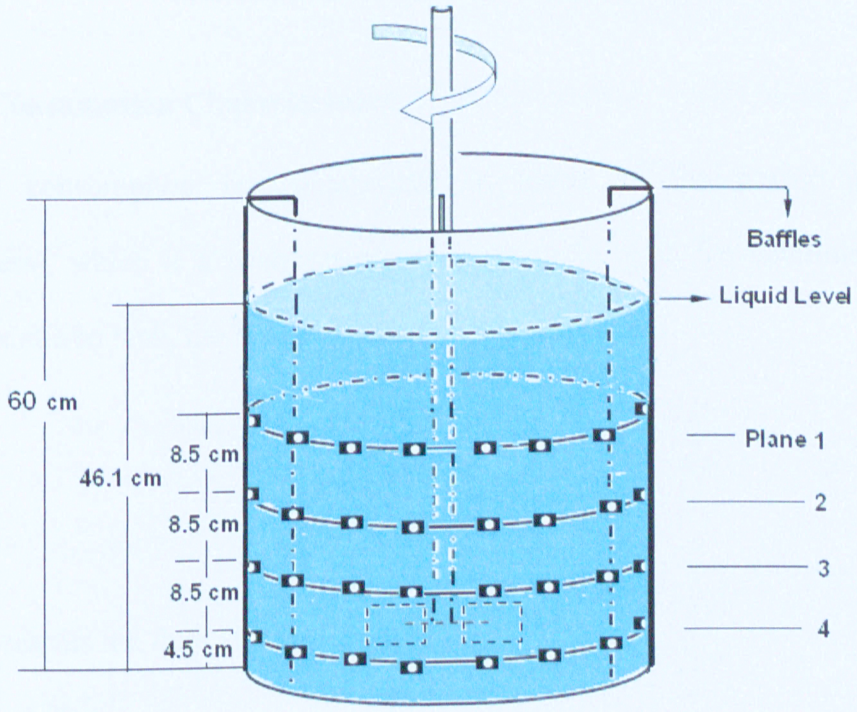

Figure 3.14 Sensing system of ERT – dimensions and spacing of four measurement planes

CHAPTER 4

RESULTS AND DISCUSSION

4.1 Power Consumption Characteristics

The power consumption is characterized in terms of the power number N_p (dimensionless), which is a characteristic of the impeller type. To determine the flow regime in the stirred tank, the Reynolds number was defined as:

$$Re = ND^2\rho/\mu \tag{4.1}$$

Where μ represents the fluid viscosity ($N{\cdot}s/m^2$).

Figure 4.1 depicts the power number (N_p) as a function of Reynolds number (Re) for RT6 and PBTU45, respectively. It shows that at high Re ($>10^4$), the flow regime was fully turbulent and the power curve became horizontal (i.e. N_p achieved a constant value). Similar observations have been made by Holland and Chapman (1966). Furthermore, these authors presented that the plot was linear (laminar flow) only at low Reynolds numbers (Re<10). Also, transition flow regime was observed at Re = 20 to 2000.

Similarly, for the impeller PBTU, it also can be observed that high Re ($> 10^4$) resulted in a fully turbulent flow condition.

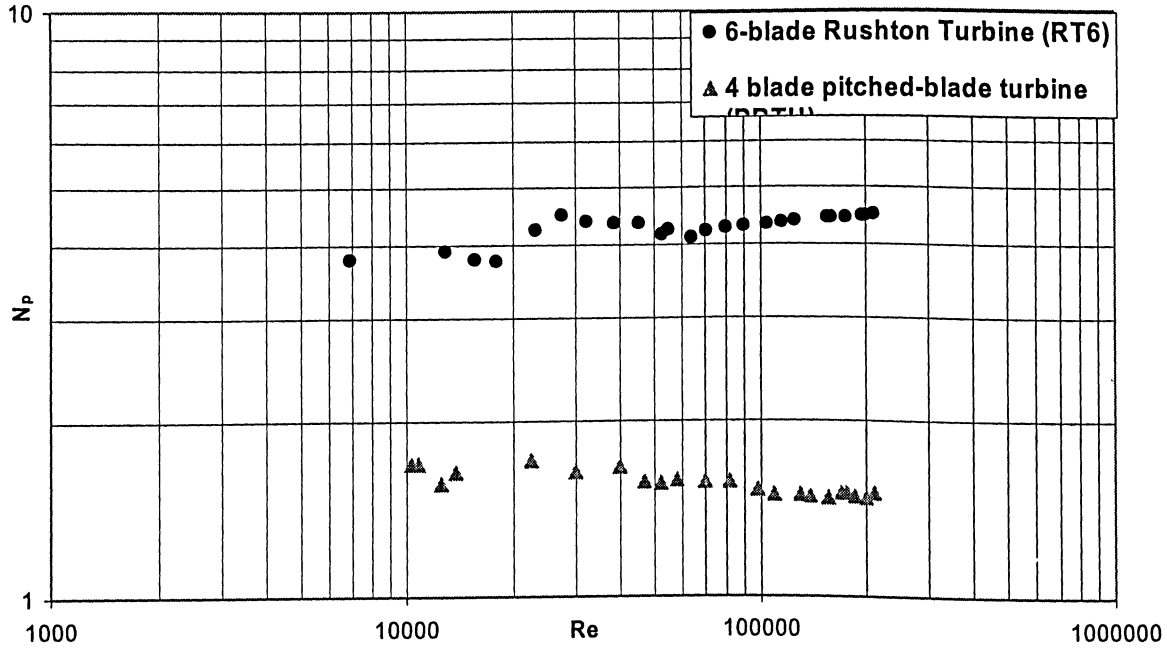

Figure 4.1 Experimental power curve for impeller RT6 and PBTU

In general, at high Reynolds numbers, when the vessel is adequately baffled, the power number N_p becomes a constant (i.e. independent of Reynolds number), and it depends only on the impeller and vessel geometry. Many studies have been carried out regarding the power curve in various geometrical tanks (Rushton et al., 1950; Bates et al., 1963; Shiue and Wong, 1984; Houcine et al., 2000). It has been noted that a slight variation of the power number can be observed by modifying the agitator's diameter or its off-bottom clearance.

The term power consumption per unit mass of liquid (P_m, WKg^{-1}) was introduced and can be obtained by the equation:

$$P_m = P/\rho V \tag{4.2}$$

Where V and ρ are volume (m^3) and density of the liquid (kg/m^3) within the tank, respectively. The combination of Equation 3.3 and 4.2 will result in:

$$P_m = N_p D^5 N^3 / V \tag{4.3}$$

From this P_m expression, Mmbaga and Bennington (1997) and Bulicco et al (1997) obtained the power number by taking a least square regression of the power input (consumption) per unit mass P_m against the cube of the impeller speed under turbulent conditions. Figure 4.2 used this method and gave the N_p of the RT 6 as 4.48. This value

was within the range of the typical values for RT 6 (N_p = 4.3 to 5.05). Similarly, the N_p for the impeller PBTU was obtained as 1.51 (typical N_p from 1.14 to 2.2) (Holland and Chapman, 1966).

The power efficiency of an impeller, the measure of the effectiveness of different type impellers, can be calculated as the ratio of the flow number to the impeller power number:

$$\eta_p = \frac{F_l}{N_p} \tag{4. 4}$$

Where η_p is energy efficiency of the impeller; F_l is flow number (sometimes called the pumping number, dimensionless); N_p is impeller power number.

In this equation, the flow number can be defined as:

$$F_l = \frac{Q}{ND^3} \tag{4. 5}$$

Where F_l is flow number; Q is the volumetric flow rate of liquid (m^3s^{-1}); N is impeller rotational speed (s^{-1}); D is the impeller diameter (m).

The flow numbers of RT6 and PBTU were obtained as 0.72 and 0.79, respectively (Rushton et al., 1950b). The power efficiency (η_p) of RT6 was calculated as 16.07% (for RPTU, η_p = 52.32%). It is very clear that impeller PBTU had a better performance

regarding power efficiency. Similar observation has been made by researchers (Rushton et al., 1950b).

4.2 ERT Measurements

An example of a typical set of tomograms after a single injection of a concentrated brine solution into the stirred tank filled with domestic tap water is shown in Figure 4.3. This figure represents a time sequence of the images depicting relative changes in the conductivity. The experiment was conducted for the radial impeller RT6 at r = 10 cm, θ = 15°, N = 250 rpm, C = 13 cm. A total of 80 frames of data were collected, each frame representing a measurement "snapshot" time of 1.1 s. The entire conductivity range was displayed using a color scale. The red color reflected the high conductivity liquid region, whereas, blue colour showed the low conductivity field. The time sequence of images showed that a homogeneous mixture was obtained after 17 s. That is, based on the conductivity relative changes, as the mixing progressed, the mixture achieved a homogenous state after 17 s.

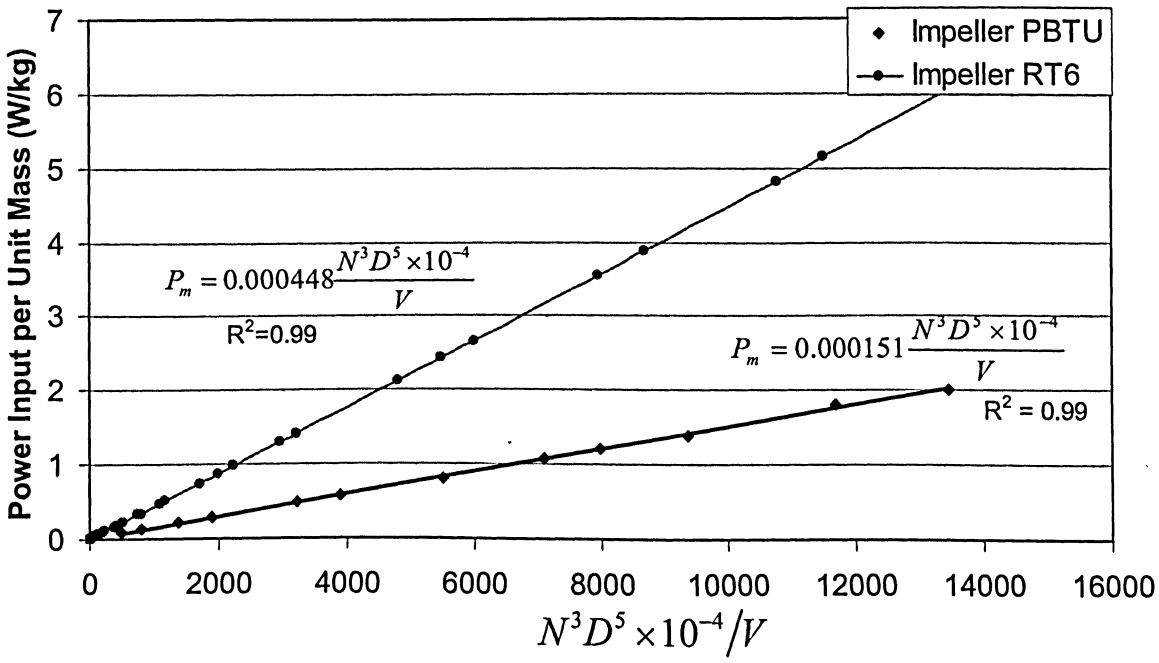

Figure 4.2 Power per unit mass (P_m) versus $N^3D^5\times10^{-4}/V$ for impeller RT and PBTU

Figure 4.4 demonstrates a clearer view for a typical tomographic image of the conductivity distribution through the measurement plane 3.

After obtaining the images by ERT, the detected conductivity data from 4 planes were instantly transformed into the concentration profile by the program itself. This procedure was performed by using the following equation which was obtained from experimental calibration (ITS System 2000 Version 5.0 Software Operating Manual):

$$c = 0.0687\sigma_{mc} - 0.1087 \tag{4.6}$$

Where c is the concentration of NaCl (g/l) and σ_{mc} is the reconstructed measured conductivity (mS/cm).

4.3 Mixing Time Studies

In Figure 4.5, as an example, the variation of the concentration profile within the tank is given. The mixing time t was calculated as the time required for the tracer concentration to reach within 100±5% of the final tracer concentration. From this graph, it is very clear that the mixing time t_{95} can be found to be 17 s for the impeller RT6 at the location of the UV tubes r = 10 cm, θ = 15° (N = 250 rpm, C = 13cm). Similar strategy was used to evaluate the mixing time for all the present experiments.

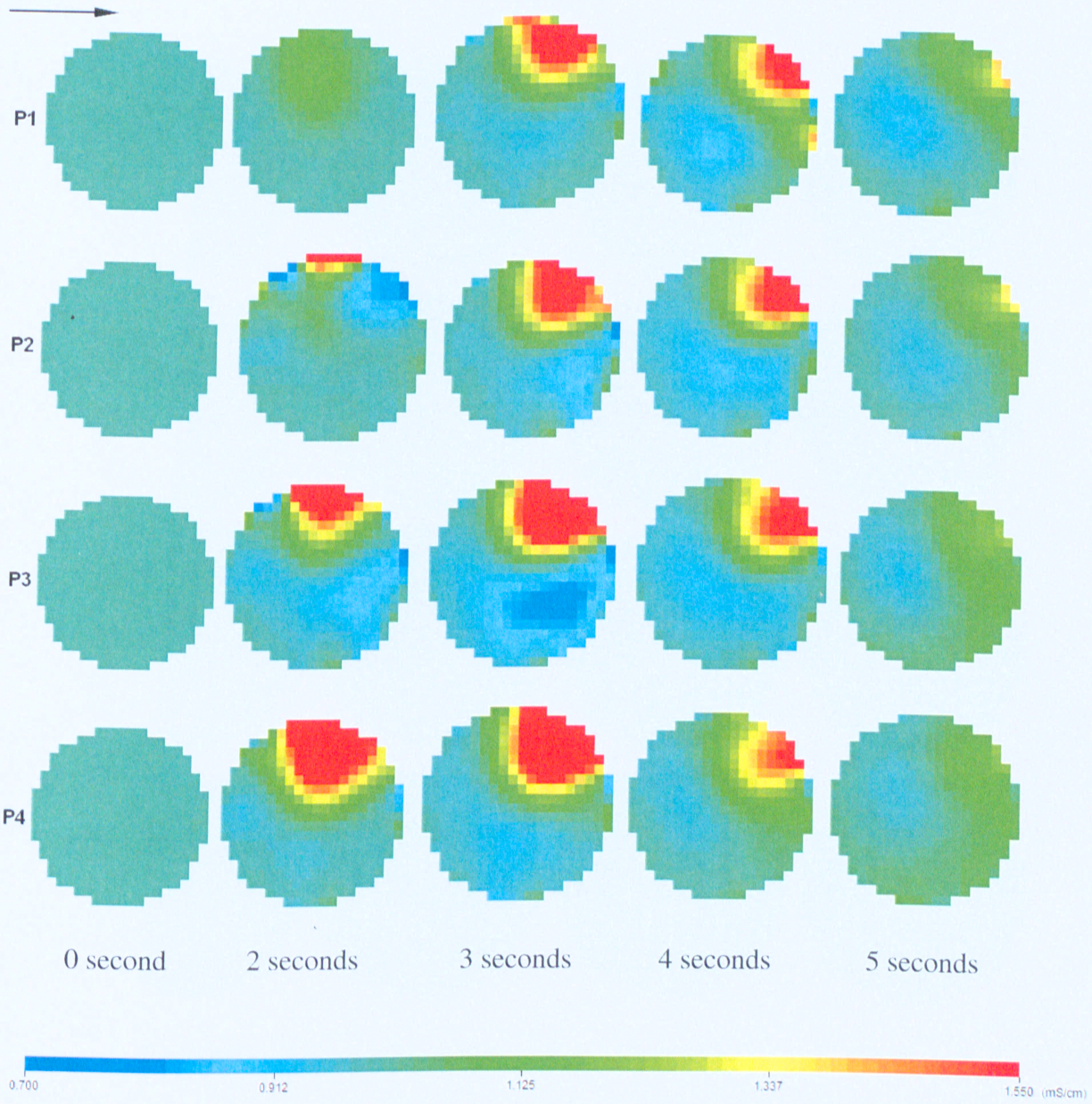
P1
P2
P3
P4
0 second
2 seconds
3 seconds
4 seconds
5 seconds
0.700
0.912
1.125
1.337
1.550 (mS/cm)

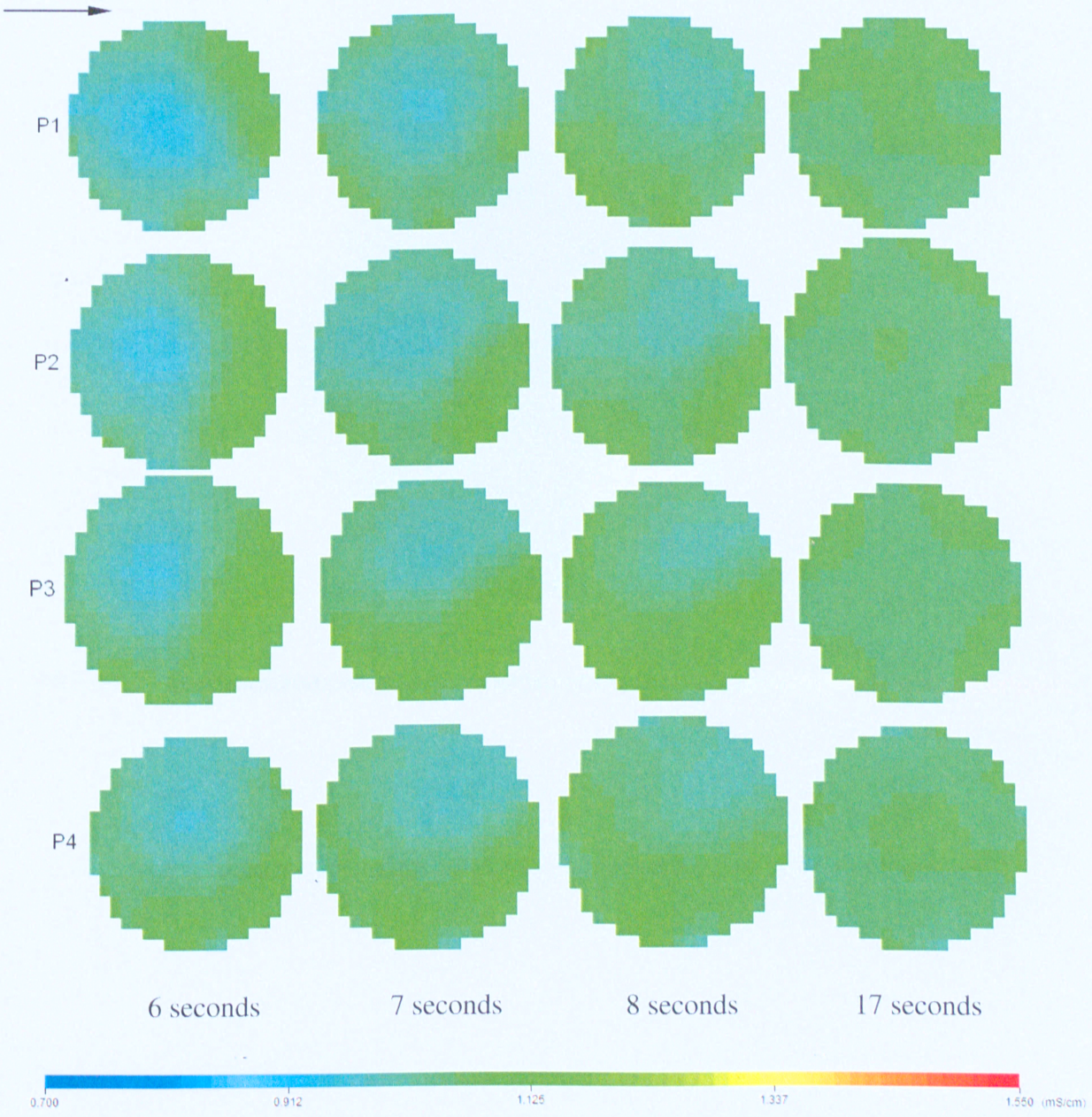

Figure 4.3 Time series of tomographic images collected from 4 measurement planes following an injection of a high-conductivity tracer for RT6 at r = 10cm, θ = 15°, N = 250 rpm, C = 13cm.

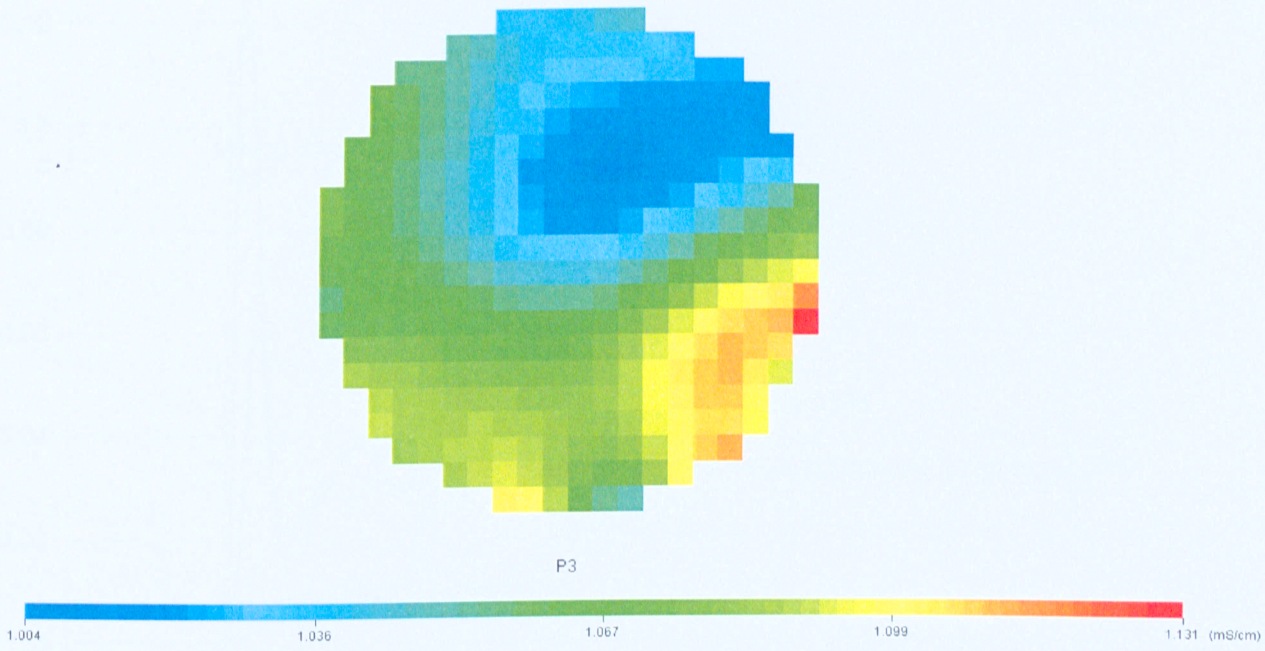

Figure 4.4 A tomographic image of conductivity distribution measured by plane 3.

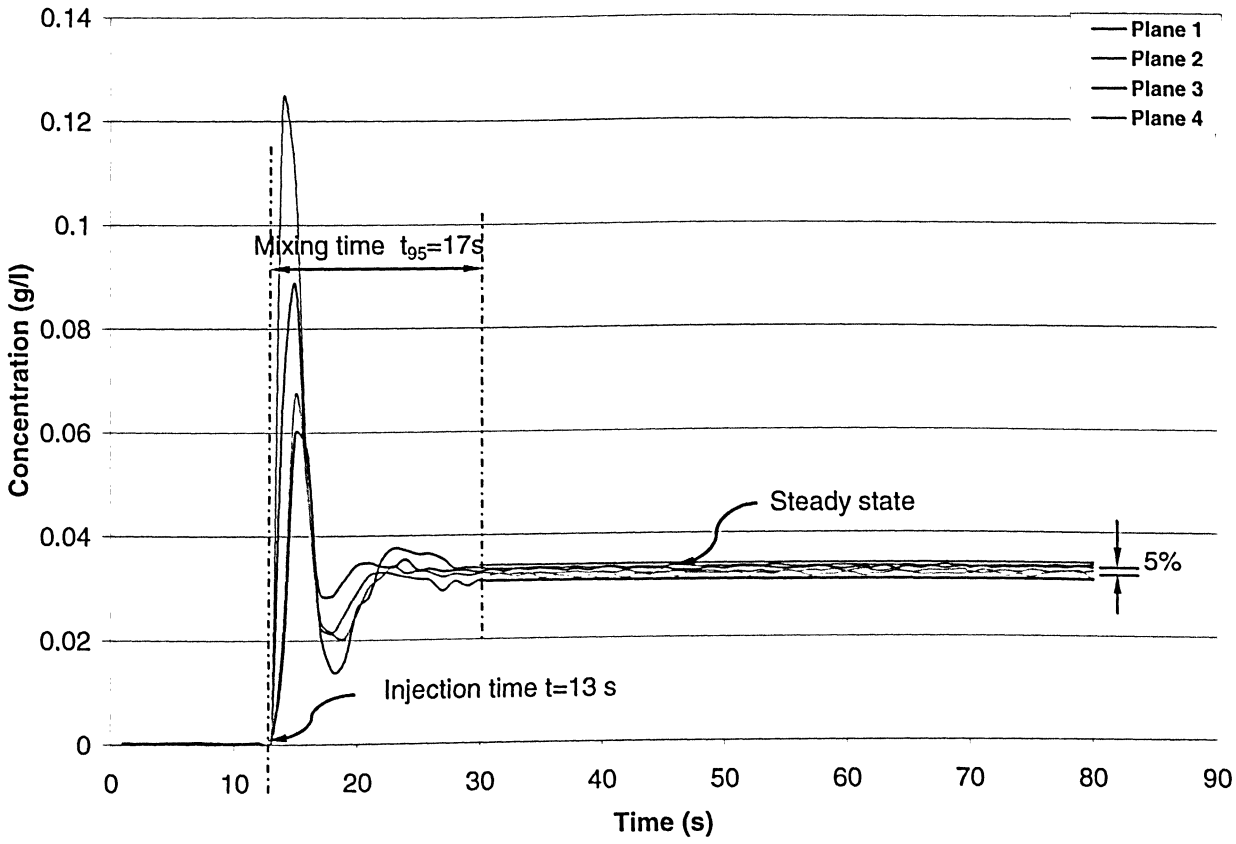

Figure 4.5 Mixing time at location of UV tubes r = 10 cm, θ = 15° (impeller RT6, N = 250 rpm, C = 13cm,)

4.3.1 Effect of locations of UV tubes

As previously described in experimental set-up (see Table 3.2), there were 18 possible locations of the UV tubes which can be chosen for each impeller rotational speed.

Figure 4.6 and Figure 4.7 show that the variation of the mixing time with the same volume of the tracer that was added for 18 different locations of the UV tubes at the rotational speed N = 45 rpm and N = 150 rpm, respectively. In these experiments, the clearance was specified as 13 cm (i.e. C = T/3) and the impeller RT6 was employed.

From Figure 4.6 and Figure 4.7, it is clear that within the fully turbulent flow regime, for the same r (i.e. 10 cm, 11.5 cm, 13cm ,14.5cm or 16 cm), the mixing time decreased considerably with an increase of the angle θ (i.e. 0°, 15°, 30° or 45 °). On the other hand, for the same angel θ=0°, the mixing time decreased with a decrease of the distance r. In Figure 4.6, the maximum mixing time in this case was found as 65 s, where the location of the UV tubes was positioned at r = 13 cm, θ = 0°. In addition, the minimum mixing time was 39s at r = 16 cm, θ = 45°. The origin of this type of behaviour probably can be speculated on the basis of the baffle location and baffle width.

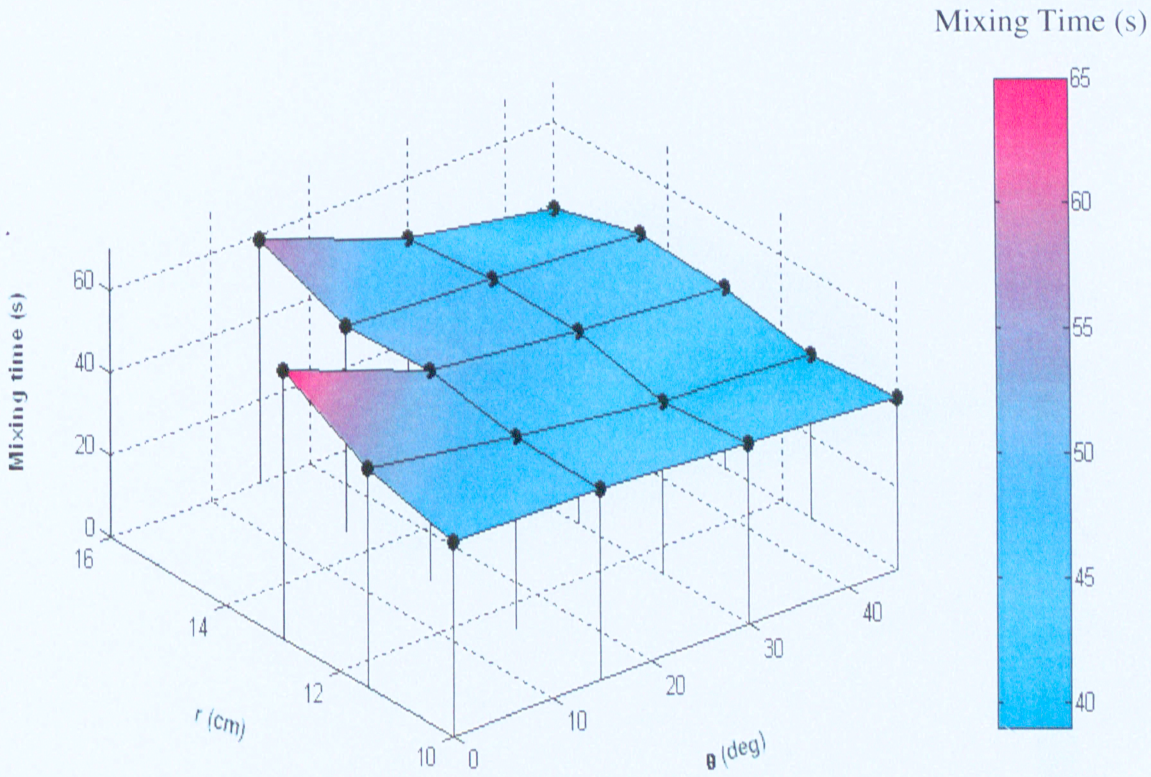

Figure 4.6 The variation of the mixing time for 18 different locations of UV tubes (impeller RT6, N = 45 rpm, C = 13cm).

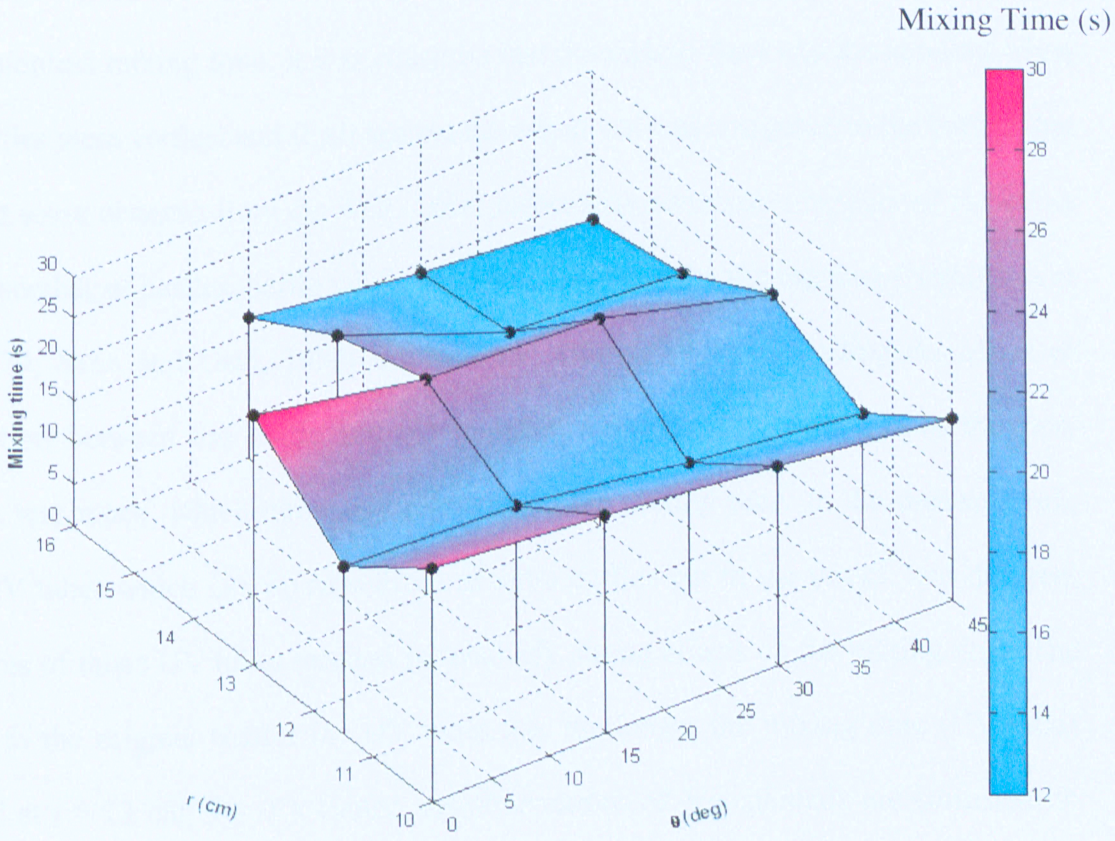

Figure 4.7 The variation of the mixing time for 18 different locations of UV tubes (impeller RT6, N = 150 rpm, C = 13cm)

Extensive investigations regarding the effect of the baffle geometry on the mixing time have been carried out. Kramers et al. (1953) investigated the effects of the baffling on the dimensionless mixing time. It was observed that the mixing time was the smallest when the baffles were vertical and flush against the vessel walls as compared to the baffles that were at some distance from the wall. Other researchers have also investigated the effect of the number of baffles, baffle width and baffle length on the mixing time (Nishikawa et al., 1979; Sano and Usui, 1987; Brennan and Lehrer, 1976), indicating the effect of interaction between the baffle and the impeller. Consequently, a change in the flow pattern was made, which ultimately reflected on the mixing time. In the present work, four UV tubes which can be considered as extra baffles put in the vessel, and different locations of those UV tubes resulted in relatively strong effects on the mixing time. The closer to the original baffles the UV tubes are, the longer the mixing time (UV tubes located at r = 13 cm, $\theta = 0°$). Hence, the observations of present study are consistent to those of previous study.

Since the accuracy of the final experimental results is of paramount importance, it was necessary to investigate the errors of the generated data. However, replication of all experiment sets is not feasible, so 36 experiments were chosen to be replicated 2 times to evaluate the reproducibility and the accuracy of the data.

Those replicated experiments were conducted under the following conditions: (1) using the impeller RT6; (2) the clearance C = 23.4cm; and (3) the rotational speed N = 45 rpm

or N = 250 rpm. For the impeller angular speed 45 rpm, the mixing time versus angle θ and radial distance r are plotted in Figure 4.8 and Figure 4.9.

From these two figures, it can be observed that the experiment data points were close to the mean value (as the standard deviation σ was rather small (<2.12), i.e. error bar is small in Figure 4.8 and Figure 4.9, indicating the error for the acquired data was small. Generally, the standard deviation is defined as:

$$\sigma = \sqrt{\frac{1}{N}\sum_{i=1}^{N}(x_{i=1} - \bar{x})^2} \tag{4.7}$$

Where σ is standard deviation; N denotes the number of samples taken; x represents the value of the random variable; and $\overline{x}$ is the average value of x. In the present study, the variable x is mixing time.

Figure 4.8 and Figure 4.9 indicate that similar behaviour was observed (compared with Figure 4.6 for impeller RT6 with the same speed N= 45 rpm at a different clearance C = 23.4 cm. The maximum mixing time t was found at the location of the UV tubes r =13 cm, θ = 0° in contrast with the minimum mixing time location at r = 16 cm, θ = 45° (Appendix: Table A.10).

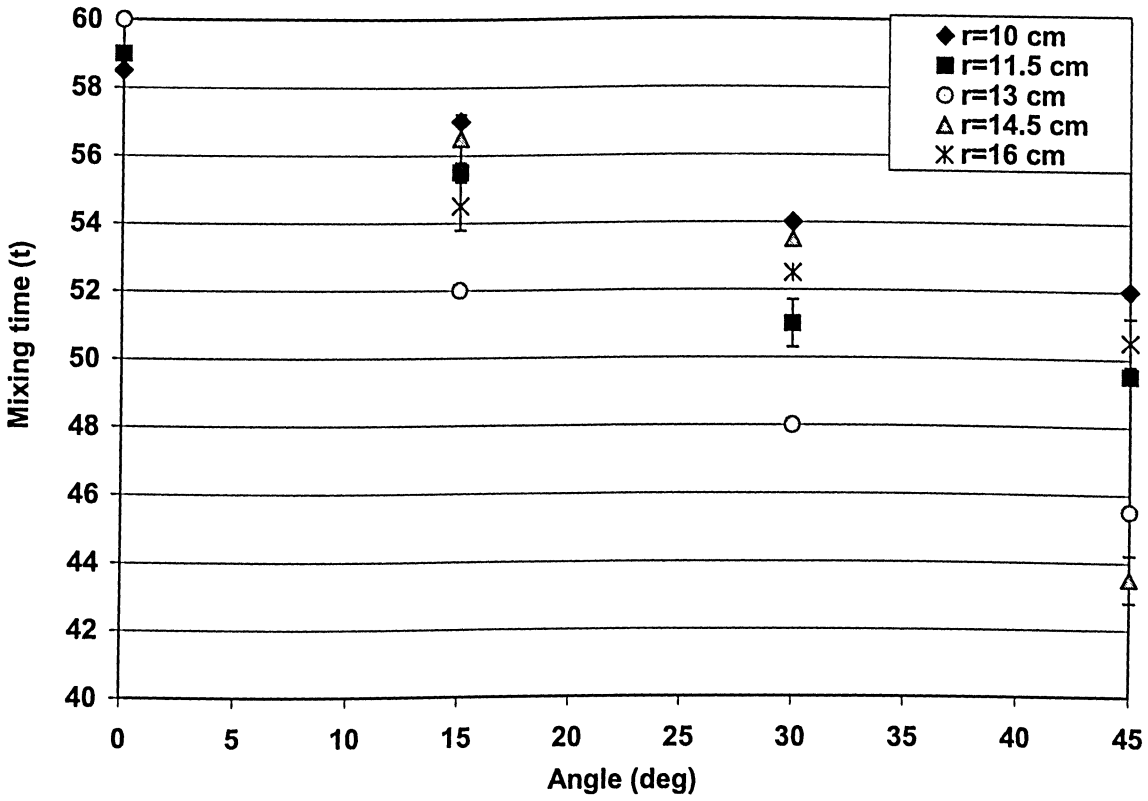

Figure 4.8 Mixing time versus angle θ (impeller RT6, N = 45 rpm, C = 23.4 cm)

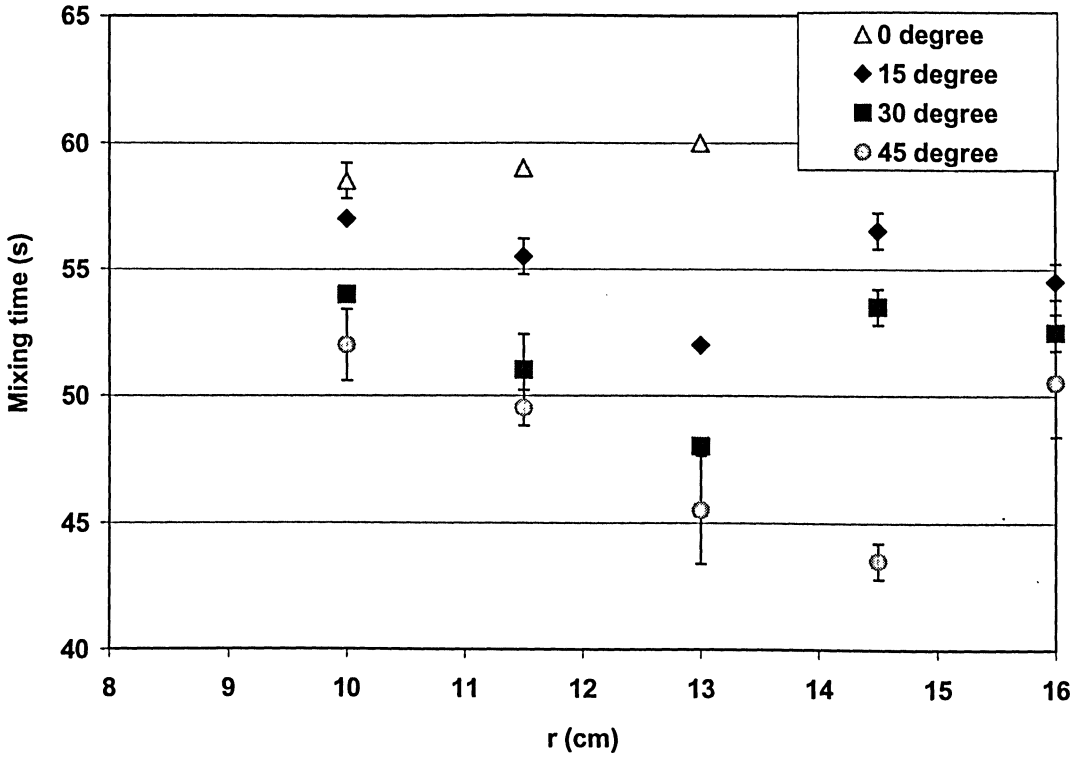

Figure 4.9 Mixing time versus radial distance r (impeller RT6, N = 45 rpm, C = 23.4 cm)

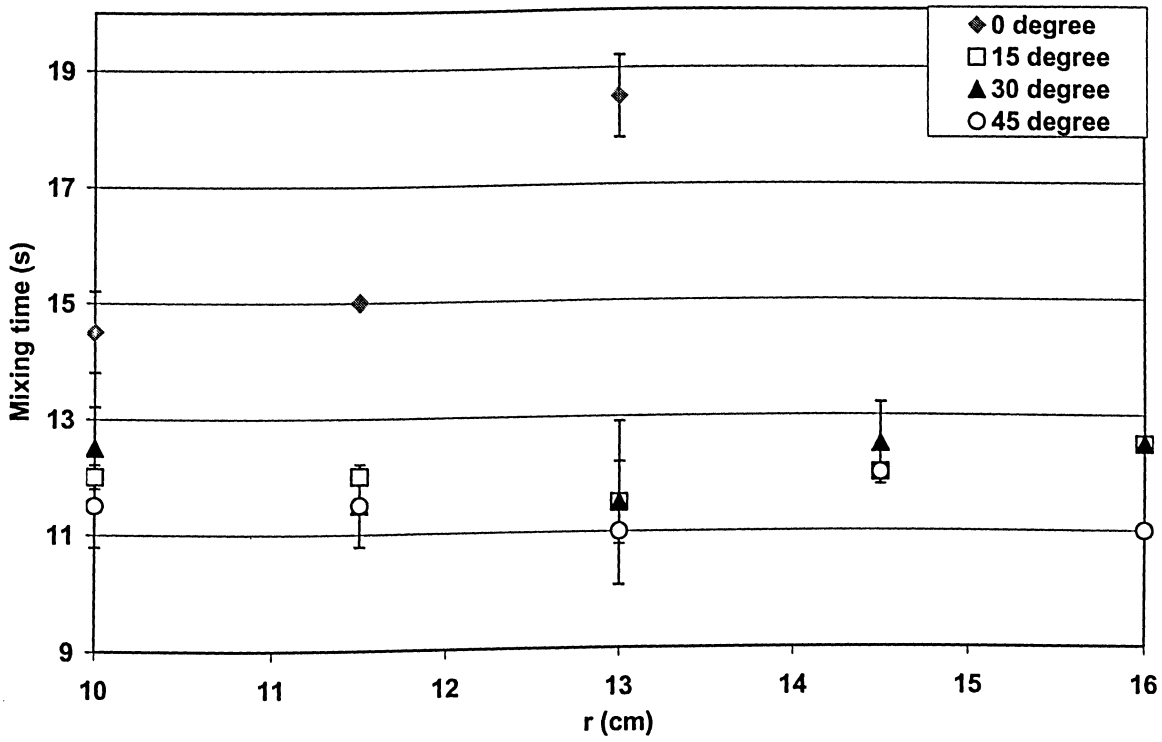
0 degree
15 degree
30 degree
45 degree
Mixing time (s)
19
17
15
13
11
9
10
11
12
13
14
15
16
r (cm)

Figure 4.10 and Figure 4.11 illustrate the mixing time variation for the impeller RT6 at N= 250 rpm with C= 23.4cm in the fully turbulent flow regime. It was observed that the maximum error of the acquired results was 1.41, and 50% of them had the minimum error of the value zero (Appendix: Table A. 11). Again, it indicates the measurement data originally collected from ERT was reliable. As can be seen from these two figures, the mixing time decreased with an increase of the angle, when having the same radial distance r. Moreover, it also implies that the effect of the location of the UV tubes on the mixing time was more pronounced at the lower speed of rotation (45 rpm) than that at the higher speed (250 pm).

In order to assess the further analysis and compare the effect of the locations of the UV tubes on the mixing time, three specific locations of the UV tubes were chosen for the evaluation. This was performed with both the radial impeller RT6 and the axial impeller PBTU at the clearance C =13 cm. Four different rotational speeds (N = 45, 250, 350, 500 rpm) were applied for both impellers. For the reason of the simplification, (1) the location of the UV tubes at r = 16 cm, angle $\theta = 45°$ was denoted as Location A; (2) the location of the UV tubes at r = 13 cm, $\theta = 0°$ was represented as Location B; (3) finally, a random chosen location of the UV tubes at r = 11.5 cm, $\theta = 30°$ was defined as Location R. From the equation 8, the power consumption per unit mass of liquid (P_m, WKg^{-1}) was calculated.

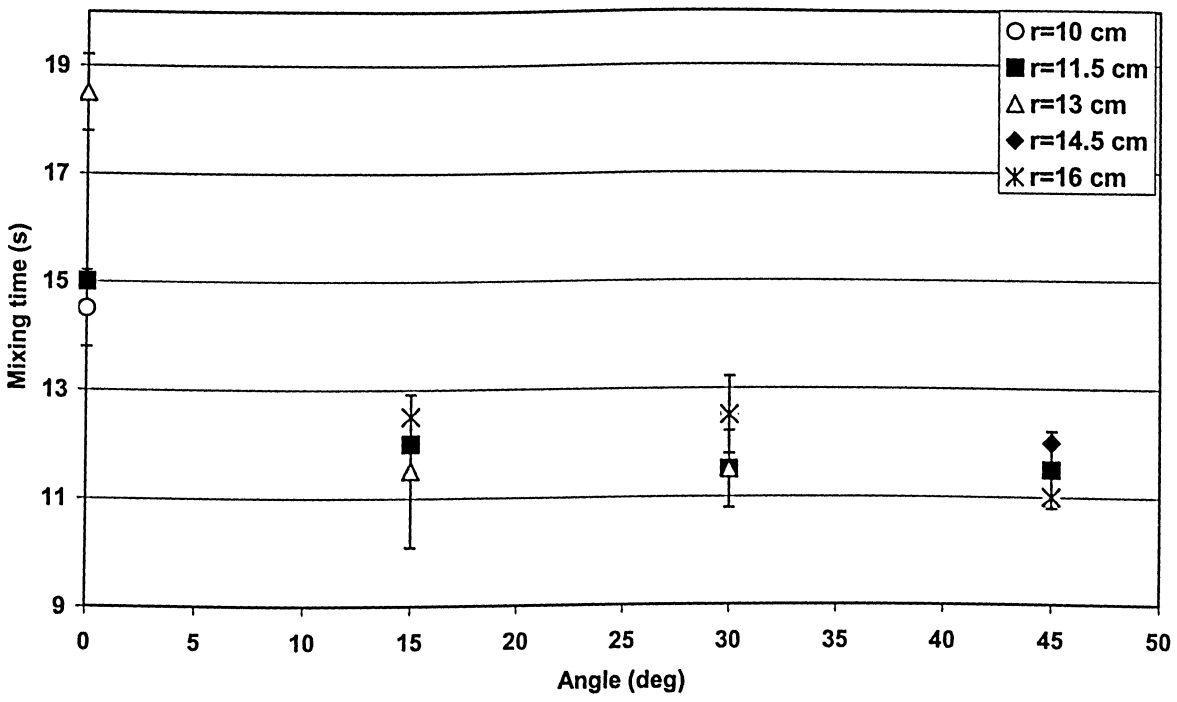

Figure 4.10 Mixing time versus angle θ (impeller RT6, N = 250 rpm, C = 23.4 cm)

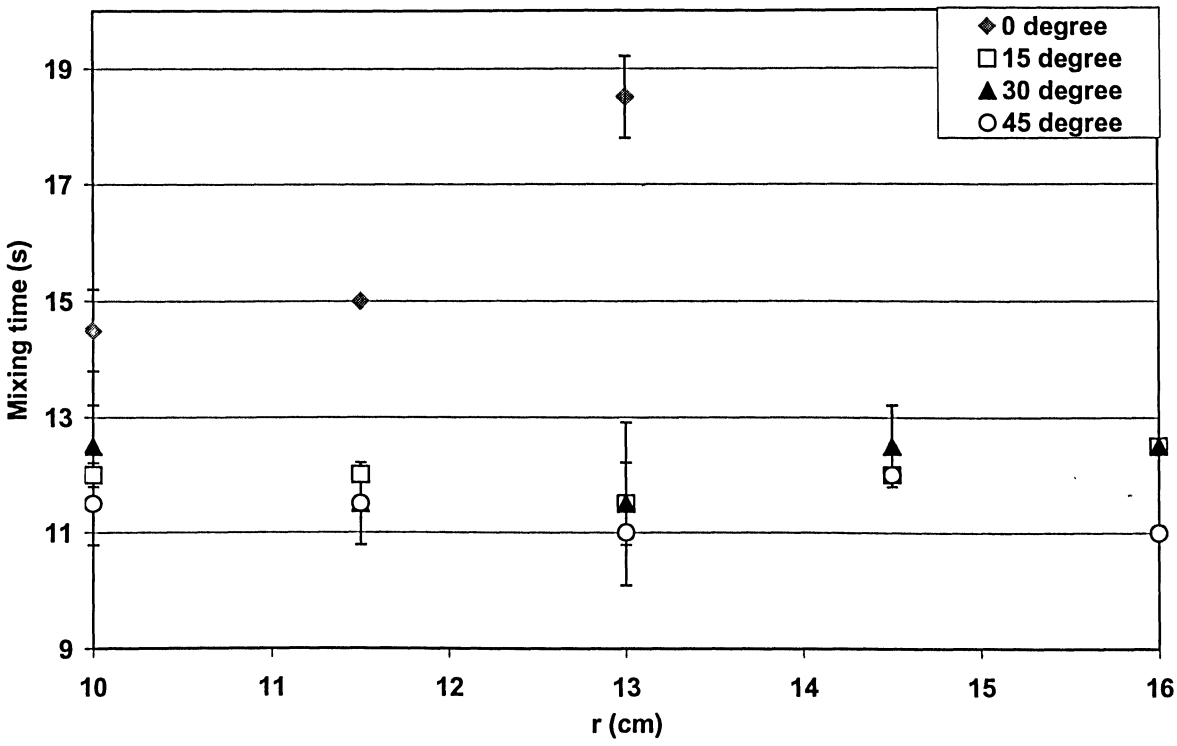

Figure 4.11 Mixing time versus radial distance r (impeller RT6, N =250 rpm, C = 23.4 cm)

In Figure 4.12, Figure 4.13, and Figure 4.14, the mixing time response curves are plotted against the power consumption per unit mass of the liquid for the impeller RT6 and PBTU. Since no study is available on the mixing time in connection with UV photoreactors using the ERT system, the results presented here are not directly comparable with those that derived from the literature.

Nevertheless, for each single location of the UV tubes, the mixing time response curve followed the similar tendency that appeared in the previous study by other authors (Houcine et al., 2000; Nere et al., 2003; Vrábel et al., 2000). These investigations mainly contributed to the mixing time study in stirred tank. The researchers have illustrated the mixing time variation against P_m with the RT and the PBTU, showing that the power consumption required by the impeller PBTU to achieve the same degree of mixing (95%) was smaller than that of RT6, similarly, as seen in Figure 4.12, Figure 4.13, and Figure 4.14. This had very good agreements with previous analysis. (From equation (**4. 4**, the power efficiency of RT6 η_p was 16.07%; η_p was 52.32% for RPTU). In addition, as anticipated in the previous analysis of the present experimental results, the maximum mixing time t was found at Location B (i.e. r = 13 cm, θ = 0°) whereas the minimum t appeared at Location A (r = 16 cm, θ = 45°).

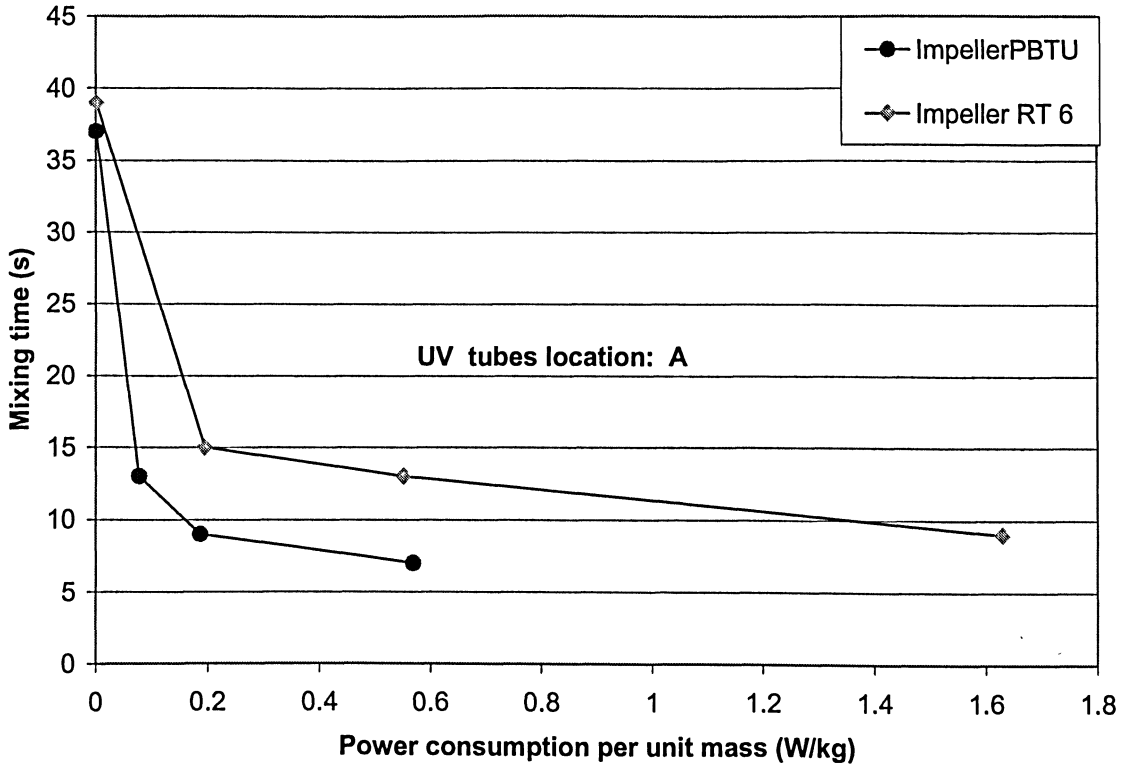

Figure 4.12 Mixing time versus power consumption per unit mass at location A (i.e. r = 16 cm, $\theta = 45°$).

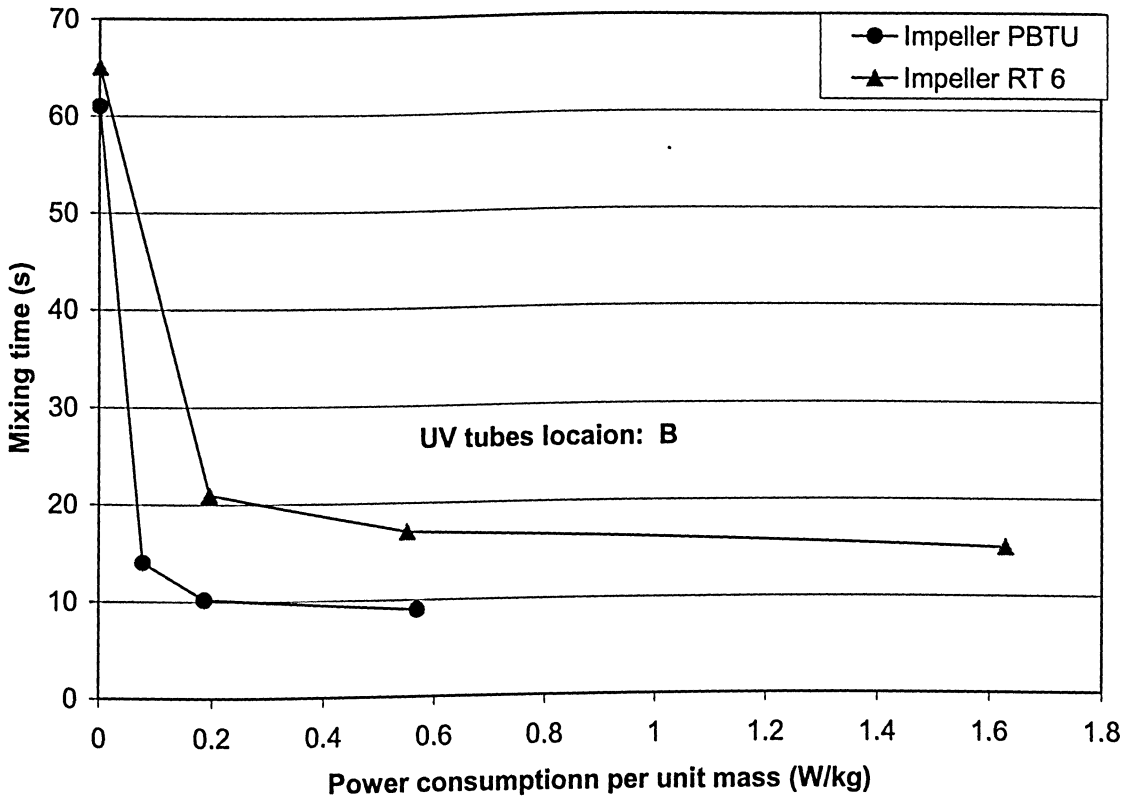

Figure 4.13 Mixing time versus power consumption per unit mass at location B (i.e. r = 13 cm, $\theta = 0°$)

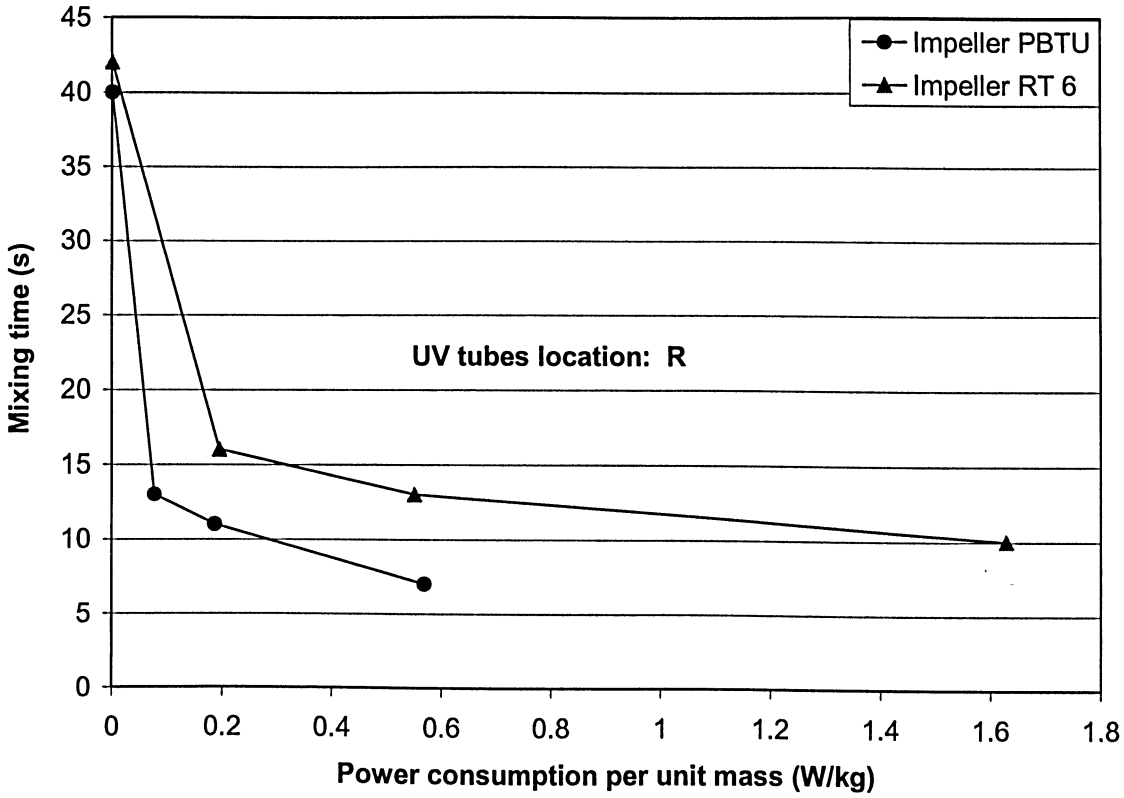

Figure 4.14 Mixing time versus power consumption per unit mass at location R (r = 11.5 cm, $\theta = 30°$).

4.3.2. Effect of Rotational Speed

The effect of the impeller rotational speed on the mixing time was studied. For the impeller RT6, the mixing time comparison at different speeds, i.e. N = 250 rpm, N = 350 rpm and N = 500 rpm are given in Figure 4.15, Figure 4.16, and Figure 4.17, respectively. In this case, the clearance was specified as 13 cm. It should also be noted that for case N = 350 rpm and N= 500 rpm, the locations of the UV tubes at r = 10 cm is not applicable due to excessive vibration of the impeller at a high rotational speed. This must be considered in order to prevent impeller from hitting the UV tubes during the tests. Otherwise, this might cause impeller breakage or the motor that run the shaft may be burned by the reason of the excessive torque.

The first observation of these tests indicates that the mixing time for the impeller RT6 varied inversely with the rotational speed N. And as expected, it also implies that the impeller rotational speed had more pronounced effects on the mixing time at the lower speed (250 rpm) than that at the higher speeds (350 rpm, 500 rpm). This type of behaviour was conceived in the previous discussion for Figure 4.6 and Figure 4.7 at RT6 rotational speed 45 rpm and 150 rpm. Similar observations have been made for the vessel equipped with dual or multiple impellers (Kasat and Pandit, 2004; Vasconcelos et al., 2000).

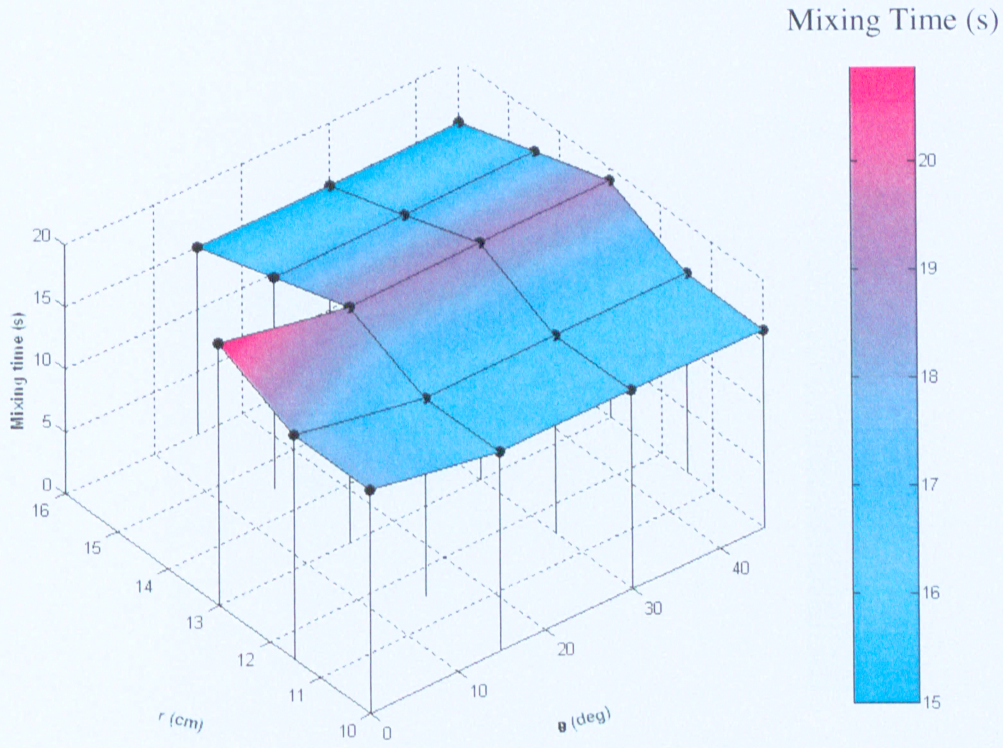

Figure 4.15 Mixing time variation at N = 250 rpm (Impeller RT6, C= 13cm)

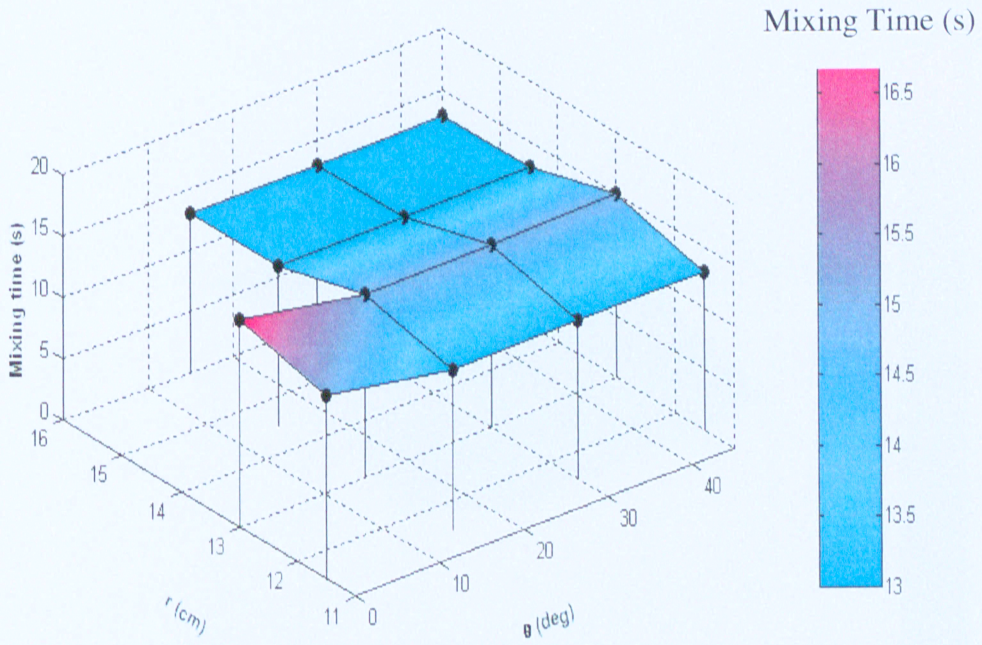

Figure 4.16 Mixing time variation at N = 350 rpm (Impeller RT6, C = 13cm)

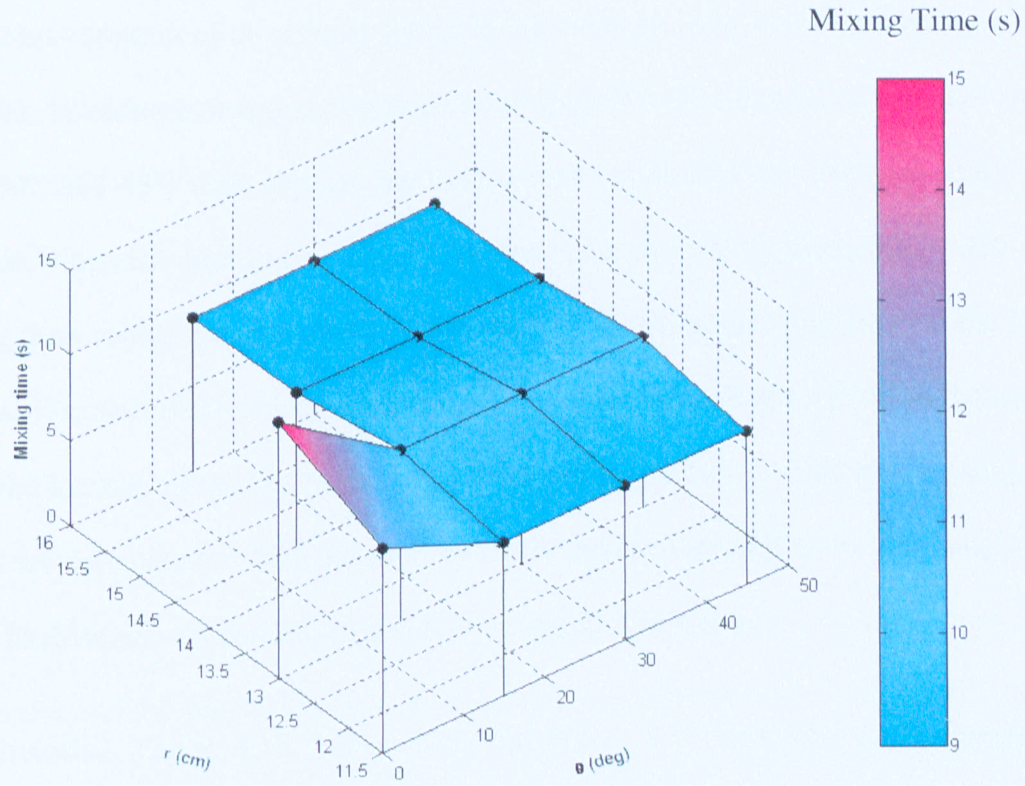

Figure 4.17 Mixing time variation at N = 500 rpm (Impeller RT6, C = 13cm)

Furthermore, from Figure 4.15, Figure 4.16, and Figure 4.17, it is very interesting to observe that with the same r, changing the angle θ from 15° to 45° will not result in significant variation of the mixing time. On the contrary, only very slight changes were obtained. In addition, it was shown that except angle θ = 0°, when all of the other angles (15°, 30°, and 45°) were applied, the mixing time approached the identical value. For instance, when the location of the UV tubes r = 13 cm was applied at N = 350 rpm, mixing time values for angle θ = 15°, 30°, and 45° were approaching close to the same, i.e. 15s, 13s, and 13s. Another example can be used to illustrate this type of the behaviour: when the location of the UV tubes r = 14.5 cm was applied at N = 500 rpm, mixing time values for the angle θ = 15°, 30°, and 45° were exactly identical as 9s. Obviously, this kind of behaviour was not observed at N = 45 or 250 rpm before.

As anticipated, Figure 4.15, Figure 4.16, and Figure 4.17 have very good agreements with the previous analysis for experiments in this study. That is, the maximum or the minimum mixing time occurred at Location B and Location A, respectively.

4.3.3 Effect of Impeller Type

A fairly large amount of the research has been carried out in regard to the effect of the impeller type on the mixing time in the literature. As previously discussed in Figure 4.12, Figure 4.13, and Figure 4.14 for the impeller RT6 and PUTU, the mixing time response clearly indicates power consumption required by the impeller PBTU to achieve the same degree of the mixing (95%) was smaller than that of RT6. Furthermore, it was observed that for a fixed geometric configuration of the tank at a same rotational speed, the

impeller PBTU had the weaker energetic needs than that of RT6. Therefore, PBTU had the better performance according to the energy efficiency.

The similar behaviour has been observed in abundant published literature that presented by many investigators (Houcine et al., 2000; Nere et al., 2003; Ogawa et al., 1980; Kumaresan and Joshi; 2006). For instance, Raghav Rao and Joshi (1988) compared the performance of various impellers, namely, RT (Rushton turbine), downflow and upflow pitched-blade turbine (PBT). The result plotting of the mixing time versus the power consumption per unit volume showed that the mixing time of RT was the highest, and the PBTD45° impeller was found to be the most energy-efficient. Rewatkar and Joshi (1991) studied the impeller RT, PBTD, and PBTU. The PBTU impeller showed a marginally higher (5-10%) mixing time, and a RT showed a considerably longer mixing time (about 50%) as compared to the impeller PBTD. They also observed that the mixing time strongly depended on the flow pattern that generated by the impeller. All of these studies showed that the impeller, which was capable of producing the top to bottom circulation at the relatively low power, were the most efficient impeller. Therefore, in general, the axial flow impeller was the most energy efficient when compared to the radial flow impeller in the case of the liquid-phase mixing. It was confirmed that the impeller design had a strong influence on the mixing time and energy efficiency.

Figure 4.18 and Figure 4.19 show the mixing time variation for the axial impeller PBTU at N= 45 rpm and N= 250 rpm. Mixing experiments were undertaken using 18 different locations of the UV tubes with the clearance C= 13cm.

When compared with Figure 4.6 (RT6, N = 45 rpm), Figure 4.18 (PBTU, N = 45 rpm) also shows that the mixing time reduced considerably with an increase of the angle θ (i.e. 0°, 15°, 30° to 45 °) with the same r. In contrast, Figure 4.19 (PBTU, N = 250 rpm) indicates the similar mixing time response tendency as Figure 4.15 (RT6, N = 250 rpm). That is, the locations of the UV tubes had much less impact on the mixing time at the higher rotational speed for both impeller RT6 and PBTU. As shown in Figure 4.18 and Figure 4.19, for the impeller PBTU, the maximum mixing time t was found at Location B (i.e. r = 13 cm, θ = 0°), and the minimum t appeared at Location A (r = 16 cm, θ = 45°). Accordingly, this behaviour showed the very good agreement with the impeller RT.

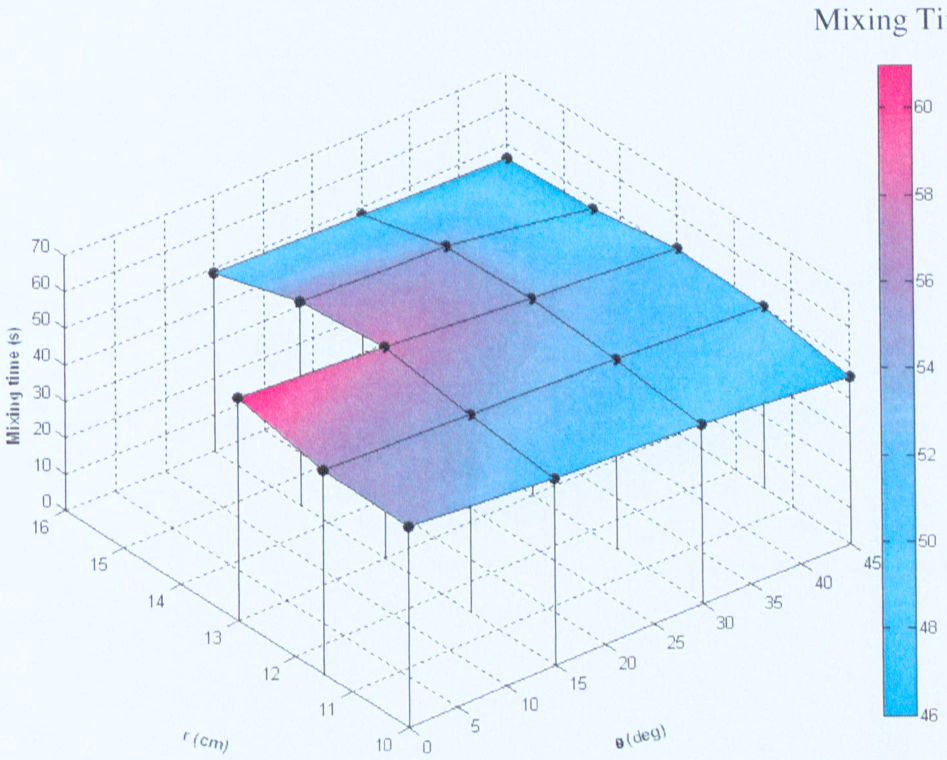

Figure 4.18 Variation of mixing time for 18 different locations of UV tubes (impeller PBTU, N = 45 rpm, C = 13cm).

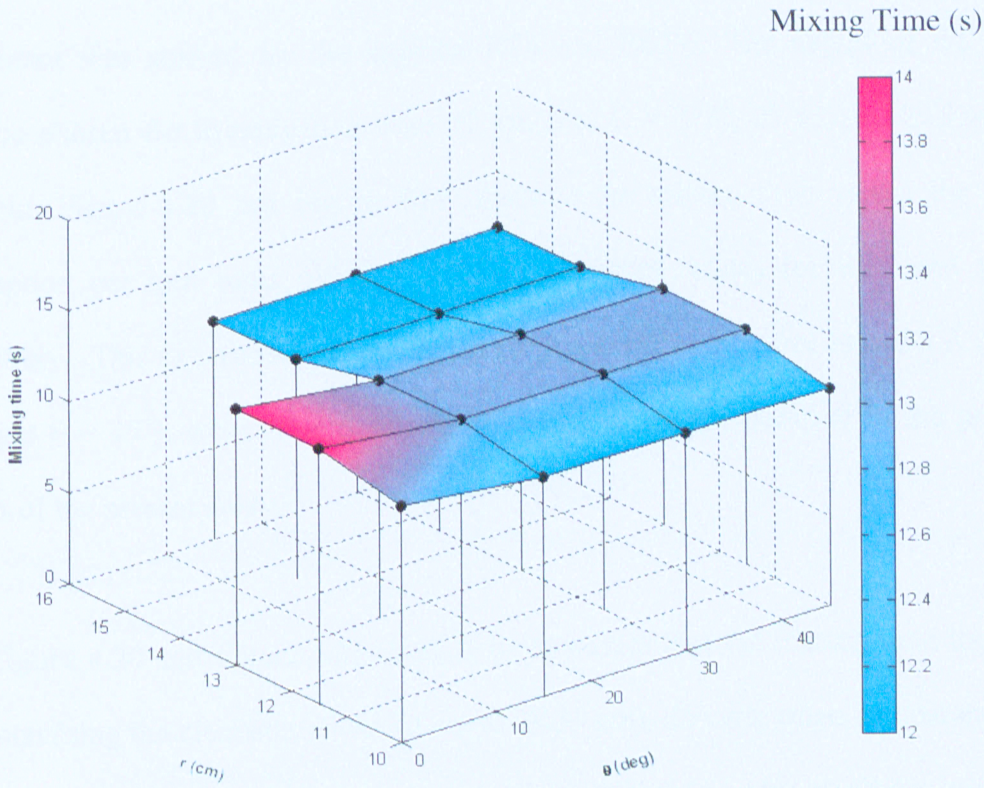

Figure 4.19 Variation of mixing time for 18 different locations of UV tubes (impeller PBTU, N = 250 rpm, C = 13cm).

4.3.4 Effect of Off-Bottom Clearance

The effect of the off-bottom clearance (denoted as C) on the mixing time in the stirred tank reactor was studied for the impeller RT6 and PBTU. The values of the stirrer clearance chosen for investigation were 13 cm (i.e. C = T/3), 21.45 cm, 29.9cm, and 38.35 cm. Figure 4.20 and Figure 4.21 illustrate the mixing time versus the power consumption per unit mass using 4 different clearance values for RT6 and PBTU, respectively. This experiments were carried for a specified UV tubes location A (r = 16 cm, angle θ = 45°), where the minimum mixing time always occurred in the previous analysis of the present study.

From Figure 4.20 and Figure 4.21, first, it is very clear that the mixing time increased when increasing the clearance (from 13 cm to 38.35 cm). Second, when compared on the equal power consumption per unit mass basis, the PBTU showed the smaller mixing time than that of RT6. Third, it was found that the mixing time was the lowest at the clearance C = 13cm (T/3) for both impeller RT6 and PBTU. Consequently, from the investigation, it can be recommended that the clearance C should be kept equal to the T/3 for both standard PBTU and RT6.

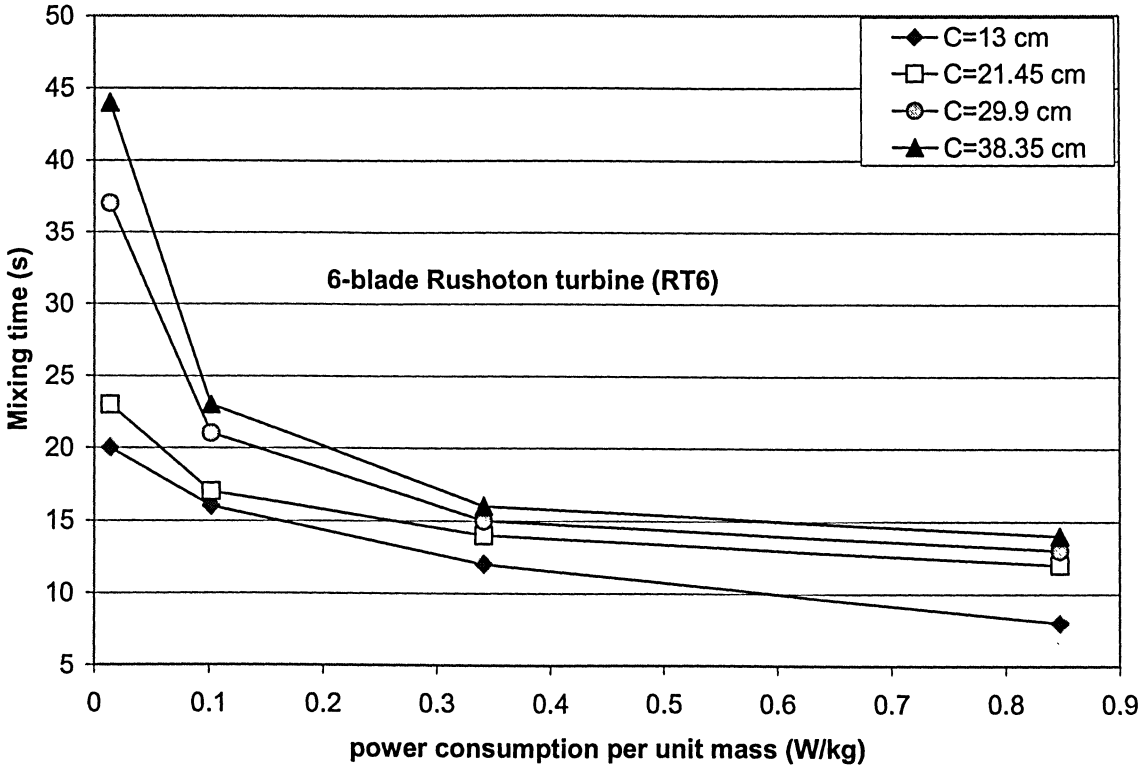

Figure 4.20 Mixing time versus power consumption per unit mass using different clearances (impeller RT6)

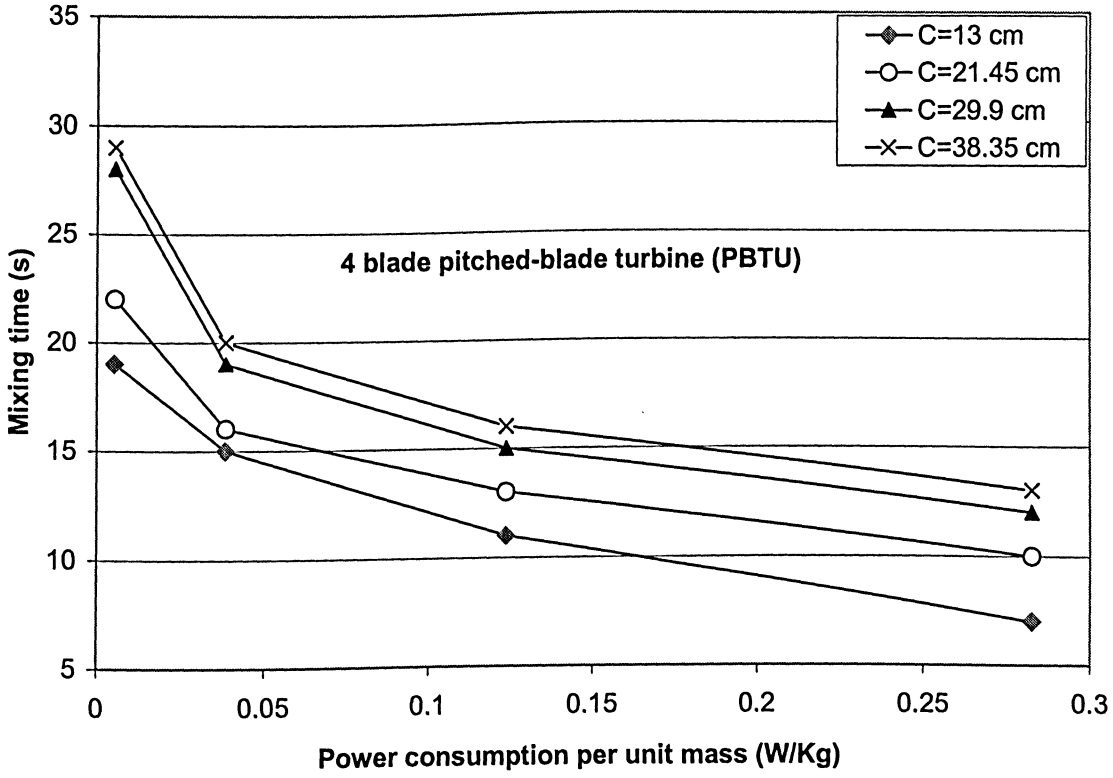

Figure 4.21 Mixing time versus power consumption per unit mass using different clearances (impeller PBTU)

Since the tendency of the mixing time variation was attributed to the overall flow pattern that generated, in turn, resulting in the consequent change in the power consumption. In the present study, different impeller clearances were used, and hence additive power behaviour was quite expected. Various researches in the literature pertaining to the clearance effect on the mixing time have been critically studied, and similar results can be seen as in line with the present work.

Raghav Rao and Joshi (1988) investigated the effect of the impeller clearance for the Rushton turbine (RT), up-flow pictched-blade turbine (PBTU), and down-flow pictched-blade turbine (PBTD). It was found that the mixing time decreased as the impeller clearance diminished in the range $T/3$ to $T/6$ for the impeller RT and PBTU. For the impeller PBTD, the effect of the impeller clearance was observed to be exactly opposite. Rewatkar and Joshi (1991) studied the effect of the impeller clearance on the mixing time for the tanks that agitated with the pitched-blade turbine (PBT) and flat-blade turbine (FBT). The value of the C/T for the several impeller designs varied. It was found that the standard PBTD45 with $C/T = 0.33$ performed best. Furthermore, they stated that the mixing time was a result of the flow pattern in the tank, resulting in the power consumption variation. Raghav Rao (1987) provided the comprehensive study regarding the effect of the clearance for different impeller designs at a wide range of the power consumption. He observed that the effect of the clearance depended on the impeller design, and the PBTD ($C = T/3$) was the most energy-efficient. Other investigations are

also available for the clearance effect study on the mixing time using RT6 and PBTU, and similar behaviour has been reported (Shiue and Wong, 1984).

CHAPTER 5

CONCLUSIONS AND RECOMMENDATIONS

5.1 Conclusions

Comprehensive data were collected for the mixing time and power consumption in the liquid phase over a wide range of the speed of rotation (100 to 500 rpm), clearance (13cm to 38.35cm), two different impeller types (RT6 and PBTU), 18 locations of the UV tubes (r varied from 10 to 16 cm; θ varied from 0° to 45°). Mixing experiments were undertaken using a promising imaging technique (ERT) to get the internal distribution of conductivity within the stirred multiple-lamp UV photoreactor. The fully turbulent liquid-phase mixing was investigated.

The foremost important point of the present study was the evaluation of the locations of the UV tubes on the mixing performance. It could be stated that the locations of the UV tubes had a significant impact on the mixing time, particularly at the lower speed of rotation (45, 150 rpm). In this case, for a given configuration of the tank with the same r (10 to 16 cm) which was the radial distance between shaft centre and UV tubes center, the mixing time varied inversely with the angle θ (0 to 45°) (θ was the angle from the UV tubes original placement to the next selected location). Moreover, it implied that giving same angel θ = 0° resulted in a decresed mixing time with r (the radial distance from the UV tube to the shaft center) diminishing. Another interesting observation was that at the higher speed of rotation (250, 350, 500 rpm) when the same r adopted, changing the angle θ from 15° to 45° only resulted in a slight variation on the mixing time (i.e.

approaching to be identical value). Consequently, this kind of behaviour demonstrated that the locations of the UV tubes had much less influence on the mixing time at the higher rotational speed (especially at 500 rpm). Finally, it could be found that the maximum mixing time t occurred when UV tubes were positioned at r = 13 cm, $\theta = 0°$ while minimum t appeared at location r = 16 cm, $\theta = 45°$.

The analysis of rotational speed influence on the mixing time was also addressed for the impeller RT6 and PBTU. The experiment results indicated that the mixing time varied inversely with the rotational speed, and this effect was more pronounced at lower speeds. On the basis of the measured power consumption per unit mass, which was required to achieve the same degree of the mixing (95%), the results obtained in this work confirmed that PBTU had a better performance according to the energy efficiency. It was proved that the axial flow impellers were the most energy efficient when compared to radial flow impellers in the case of liquid-phase mixing. In view of this, the impeller design had a strong influence on the mixing time and the efficacy in the mixing process.

The off-bottom clearance effect on the mixing time was studied in the present work. It was observed that the mixing time was increased when the clearance was increased (from 13 to 38.35 cm). Furthermore, the shortest mixing time occurred at the clearance C = 13cm (T/3) for both impeller RT6 and PBTU. Thus, from the present investigation, a recommendation can be made in regard to the clearance value, that is, the clearance C should be kept equal to T/3 for both standard PBTU and RT6.

5.2 Recommendations

Further investigation could be anticipated with respect to estimation of the mixing time and the power consumption using ERT as the measurement technique. The following considerations are recommended as attempt options for the future work.

Examining the influence of the impeller design on the mixing characterization by alternating impeller parameters (e.g. diameter, blade number, blade width and height, discharge angle), or by employing other types of stirrers (such as, the flat blade turbine (FBT), Lightnin A310, or marine-blade propeller). In addition, dual or multiple impellers system can also be proposed for the mixing performance study.

It is also suggested to estimate the presence or absence of the baffles, baffle number, geometry, position and draft tube influence on the mixing time and power dissipation efficiency for the present multi-lamp UV photoreactor.

Another future work recommendation could be the mixing time studies in a continuous stirred tank reactor (CSTR) of UV disinfection processes.

Furthermore, besides experimentation, developing a computational fluid dynamics (CFD) model for UV photoreactor can be also taken into account.

Finally, in view of the complex interdependency of the parametric space, it is also promising to employ dynamic modeling to screen for an optimum configuration for the impeller design, tank diameter, impeller location, baffle configuration, draft tube, etc.

NOMENCLATURE

a	impeller blade width, m
b	impeller blade height, m
B	baffle width, m
c	concentration, Kgm^{-3}
C	impeller clearance, m
D	impeller diameter, m
F_l	impeller flow number, dimensionless
h	impeller disk thickness, m
H	static liquid height, m
H_0	fluence, J/m^2
h_l	impeller blade thickness, m
H_l	tank height, m
I^*	radiation (or light) intensity, Wcm^{-2}
K	the rate constant of microorganism inactivation, dimensionless
L	baffle length, m
N	impeller rotational speed, rps
N_p	power number of the impeller
N_t	the number of microorganisms at time t
$N_{t=o}$	the number of microorganisms before UV radiation
P	power, W

P_m	power consumption per unit mass of liquid, W Kg^{-1}
r	radial distance between UV tubes and shaft center, m
S	spacing (distance) between impellers, m
t	mixing time, s
T	tank inner diameter, m
t_{95}	mixing time to 5% deviation from homogeneity, s
t_M	the mean residence time, s
t_R	reaction time, s
V	volume of liquid in the tank, m^3

Greek Symbols

β	discharge angle of impeller, deg
ε_{avg}	power consumption per unit mass, W/Kg
η_p	energy efficiency of the impeller, %
θ	angle from the UV tubes original placement to the next selected location, deg
λ	wavelength, nm
μ	fluid viscosity, $N \cdot s/m^2$
ρ	fluid density, kg/m^3
σ	standard deviation
σ_{mc}	reconstructed measured conductivity, ms/cm
τ	torque, $m \cdot N$
ω	angular speed, radians/s

Abbreviations

AOPs	advanced oxidation processes
AOTs	advanced oxidation technologies
AOX	adsorbable organic halogen
CFD	computational fluid dynamics
CFU	colony forming units
CSTR	continuous stirred tank reactor
DT	disk turbine (flat blade disk turbine, same as RT)
EOPs	enhanced oxidation processes
FBT	flat-blade turbine
HPC	heterotrophic plate count
PBT	pitched-blade turbine
PBTD	pitched-blade downflow turbine
PBTU	pitched-blade upflow turbine
RT	Rushton turbine (flat blade disk turbine)

REFERENCES

Abdullah, M.Z., Dyakowski, T., Dickin, F.J., Williams, R.A., Observation of hydrocyclone separator dynamics using resistive electrical impedance tomography, Proc. European Concerted Action on Process Tomography, Karlsruhe, 25-27 Manchester, pp. 93-96, 1993.

Bates, R. L., Fondy, P. L., Corpstein, R. R., An Examination of some geometric parameters of impeller power. Ind. Eng. Chem.Process Des. Dev. 2, pp. 310-314, 1963.

Bates, R. L., Fondy, P. L., Fenic, J. C., Impeller characteristics and power in mixing; Uhl, V. W.; Gray, J. B., Eds.; Academic Press: New York, Vol. I, pp. 111-178, 1966.

Beck, M.S., Williams, R.A., Process tomography: A European innovation and its applications, Measure. Sci. and Technol. 7 (3), pp. 215-224, 1996.

Biey, E.M., Verstraete. W., The use of a UV lamp for control of odor decomposition of kichen and vegetable waste, Environ. Technol. 20, pp. 331-335, 1999.

Biggs, R.D., Mixing rates in stirred tanks, AIChE J. 9, pp. 636-640, 1963.

Block S.S., Disinfectants and antiseptics, in: Kirk-Othmer Vol. 8, pp. 237-292, John Wiley & Sons, New York, 1993.

Bolton, G. T., Hooper, C. W., Mann, R.; Stitt, E., Flow distribution and velocity measurement in a radial flow fixed bed reactor using electrical resistance tomography. H. Chem. Eng. Sci. 59(10), pp. 1989-1997, 2004.

Bolton, Gary T., and Primrose, Ken M., An overview of electrical tomographic measurements in pharmaceutical and related application Areas, AAPS PharmSciTech 6 (2), Article 21, 2005.

Bolton, J.R., Valladares J.E., Zanin J.P., Cooper E.J., Nickelsen M.G., Iajdi D.C., Waite T.D., Kurucz C.N., Figures-of-merit for Advanced Oxidation Technologies: a comparison ho homogeneous UV/h2o2, Heterogeneous UV/TiO2 and electron beam processes, J. Adv.Oxid.Technol.3, No.2, pp. 174-181,1998.

Braun, André, M., Maurette, Marie-Thérèse, Oliveros, Esther, Photochemical technology, Torono, John Wiley & Sons, 1991.

Brennan, D. J., Lehrer, I. H., Impeller mixing in vessels experimental studies on the influence of some parameters and formulation of a general mixing time equation, Trans. Inst. Chem. Eng. 54, pp.139-152, 1976.

Chudacek, M. W., Impeller power numbers and impeller flow numbers in profiled bottom tanks. Ind. Eng. Chem. Process Des. Dev. 24, pp. 858-867, 1985.

Clancy, J.L., Hargy, T.M., Marshall, M.M., Dyksen, J.E., UV light inactivation of Cryptosporidium oocysts. J. Am. Water Works Assoc. 90 (9), pp. 92–102, 1998.

Cory, G. P., J. C., Waterfall, R. C., A six-electrode local probe for measuring solids velocity and volume fraction profiles in solids-water flows. Lucas Measure. Sci. and Technol. 11(10), pp. 1498-1509, 2000.

Demidov, D.A., Krasnochub, A.V., Shepelin, A.V., Experimental study of the distribution function of water residence time in disinfection plants, Water Resources 28 (4), pp. 466-468, 2001.

Dickin, F., Wang, Mi., Electrical resistance tomography for process applications. Measure. Sci. & Technol. 7(3), pp. 247-60, 1996.

Dohan, J.M., Masschelein, W.J., The photochemical generation of Ozone: present state-of-the-art, Ozone Sci. Eng. 9, pp. 315-334, 1987.

Dussert, B.W., Essential criteria for selecting an: Ultraviolet disinfection system, Journal / American Water Works Association 97 (7), pp. 52-58, 2005.

Dyakowski, T., York, T., Mikos, M., Vlaev, D., Mann, R., Follows, G., Boxman, A., Wilson, M., Imaging nylon polymerisation processes by applying electrical tomography, Chem. Eng. J. 77 (1-2), pp. 105-109, 2000.

Gaskey, S., P. Vacus, T. David, J. Villermaux J.C. André, A method for the study of turbulent mixing using Fluorescence Spectroscopy, Exp. Fluid 9, pp. 137-147, 1990.

Geselowitz, D.B., An application of electrocardiographic leadd theory to impedance plethysmography, IEEE Trans. Biomed. Eng., BME-S8, pp. 38-41, 1971.

Giona, M., Paglianti, A., Cerbelli, S., Pintus, S., Adrover, A., Tracer dispersion in stirred tank reactors: Asymptotic properties and mixing characterization, Can. J. Chem. Eng. 80 (4), pp. 580-590, 2002.

Glaze WH, Kang J-W, Chapin DH., The chemistry of water treatment processes involving Ozone, Hydrogen Peroxide and Ultraviolet radiation, Ozone, Sci. Eng. 9, pp. 335-352, 1987.

Gottschalk, C.,Libra, J.A., Saupe, A., Ozonation of water and waste water, Liley-VCH, Weinheim, 2000.

Gray, D. J., Treybal, R. E., Barnett, S. M., Mixing of Single and Two Phase Systems: Power Consumption of Impellers. AIChE J. 28, pp. 195-199, 1982.

Grieve BD., Dyakowski T., Mann R., Wang M. Interfacing of EIT into an industrial pressure filter: a practical example. Proceedings of the 1st World Congress on Industrial Process Tomography, Buxton, UK, April 14-17, 1999.

Harke H-P, Disinfectants, in: Ullmann's Encyclopedia of industrial chemistry, Vol. A 8, pp. 551-563, VCH, Weinheim, 1987.

Henry, V., Helbronner, A., Recklinghausen, M., Nouvelles recherches sur la sterilization de grandes quantited d'eau par les rayons ultraviolets. Comp. Rend. Acad. Sci. 151, pp. 677–680, 1910.

Hiby, J.W., Definition and measurement of the degree of mixing liquid mixtures, Intern. Chem. Eng. 21, pp. 197-204, 1981.

Hijnen, W.A.M., E.F., Beerendonk, G.J., Medema, Inactivation credit of UV radiation for viruses, bacteria and protozoan (oo)cysts in water: A review, Water research 40, pp.3-22 , 2006.

Holden, P.J., Wang, M., Mann, R., Dickin, F.J., Edwards, R.B., Imaging stirred-vessel macromixing using electrical resistance tomography, AIChE Journal 44 (4), pp. 780-790, 1998.

Holland, F.A., Chapman, F.S., Liquid mixing and processing in stirred tanks, New York, Reinhold Pub. Corp., 1966.

Holmes, D.B., R.M. Voncken and J.A. Dekker, Fluid flow in turbine stirred, baffled tanks-I: Circulation time, Chem, Eng. Sci, 19, pp. 201-208, 1964.

Hou, Y.Y., Wang, M., Holt, R., Williams, R.A., A study of the mixing characteristics of a liquid magnetically stabilised fluidised bed using electrical resistance tomography, in: Proceedings of the Second World Congress on Industrial Process Tomography, Hannover, Germany, 29–31, pp. 315–323, 2001.

Houcine I., E. Plasari, and R. David, Effects of the stirred tank's design on power consumption and mixing time in liquid phase, Chem. Eng. Technol. 23, 7, pp. 605-613, 2000.

Hoyer, O., Anforderungen an UV-anlagen zur trinkwasserdesinfection, bbr, Wasser Tohrbau 47, No. 12, pp. 12-19, 1996.

Hoyer, O., Water disinfection with UV radiation—requirements and realization. In: Proceedings of the European Conference UV Karlsruhe, UV radiation, Effects and Technologies, September 22–24, 2003, Karlsruhe, 2004.

Hudcova, V., Machon, V., Nienow, A. W., Gas-liquid dispersion with dual Rushton Turbine impellers. Biotechnol. Bioeng, 34, pp. 617-628, 1989.

Hunter G., The history of UV disinfection in the last 20 years, IUVA News 2, No.3, pp. 5-7, 2000.

Jahoda, M., Machon, Vaclay, Homogenization of liquids in tanks stirred by multiple impellers, Chem. Eng. Technol. 17(2), pp. 95- 101, 1994.

Janex, M.L., Savoye, P., Do-Quang, Z., Blatchley III, E., Laîné, J.M., Impact of water quality and reactor hydrodynamics on wastewater disinfection by UV, use of CFD modeling for perfrmance optimization, Wat. Sci. Technol. 38, pp. 71-78, 1998.

Jia, X., Willliams R.A., Dickin F.J., McKee S.L., Development of a PC-based electrical resistance tomography visualisation data bank for design of slurry mixers, in: M.S. Beck et al. (Eds.), Process Tomography—1995, Implementation for Industrial Processes, UMIST Publications, Manchester, pp. 371–380, 1995.

Kaminoyama, M., Taguchi, S., Misumi, R., Nishi, K., Monitoring stability of reaction and dispersion states in a suspension polymerization reactor using electrical resistance tomography measurements, Chem. Eng. Sci. 60 (20), pp. 5513-5518, 2005.

Kasat, Gopal R., and Aniruddha B. Pandit, Mixing time studies in multiple impeller agitated reactors, Can. J. Chem. Eng., Vol.82, pp. 892-904, 2004.

Kotre, C.J., A sensitivity coefficient method for the reconstruction of electrical impedance tomograms, Clin.Phys. Physiol. Means., 10 (3), pp. 275-281, 1989.

Kramers, H., Baars, G. M.; Knoll, W. H. A Comparative study on the rate of mixing in stirred tanks. Chem. Eng. Sci. 2, pp. 35-42, 1953.

Kruithof, J.C., Van der Leer, R.C., Hijnen, W.A.M., Practical experiences with UV disinfection in The Netherlands, J Water SRT-Aqua 41 (2), pp. 88–94, 1992.

Kuboi, R., Nienow, A. W., The power drawn by dual impeller systems under gassed and ungassed conditions. Proc. 4th Eur.Conf. Mixing, pp. 246-261; Paper G2, 1982.

Kumaresan, T., Jyeshtharaj B. Joshi, Effect of impeller design on the flow pattern and mixing in stirred tanks, Chem. Eng. J. 115, pp. 173–193, 2006.

Labas, Marisol D., Rodolfo J. Brandi, Carlos A. Mart'ın, Alberto E. Cassano, A contribution to the UV dose concept for bacteria disinfection in well mixed photoreactors, Chem. Eng. J. 116 (3), pp. 197-202,2006.

Landau,J., Prochazka,J., Homogenization. of Miscible. Liquids, Coll.Czech. Chem Commun ,26, pp. 2961-2973,1961.

Lazarova, V., Savoye, P., Janex, M.L., Blatchley III E.R., Pommepuy, M., Advance wastewater disinfection technologies: state of the art and perspectives, Wat. Sci. Technol. 40, No. 4-5, pp. 203-213, 1999.

Legrini, O., Oliveros, E., Braun, A.M., Photochemical processes for water treatment Chemical Reviews, 93 (2), pp. 671-698, 1993.

Leitner, K.V., N., Le Bras, E., Foucault, E., Bousgarbiès, J.-L. A new photochemical reactor design for the treatment of absorbing solutions, Wat. Sci. Technol., 35 (4), pp. 215-222, 1997.

Leitzek, O., Schulte. P., Gilbert, E., Eriweiterte oxidationsverfahren in der trink-wasseraufbereitung, gwf-Wasser/Special 137, No. 14: S173-S177, 1996.

Li, L., Wei, J., Three-dimensional image analysis of mixing in stirred vessels, AIChE Journal 45 (9), pp. 1855-1865, 1999.

Lu, W.M., Yao, C.L., Gas Dispersion in a multi-stage impeller stirred tank, Proc. 7th Eur. Conf. Mixing 2, pp. 351-357, 1991.

Lucas, G.P., Cory, J., Waterfall R.C., Loh W.W., Dickin F.J., Measurement of the solids volume fraction and velocity distributions in solid– liquid flows using dual-plane electrical resistance tomography, Flow Meas. Instrum. 10, pp. 249–258, 1999.

Mann, R., Electric process tomography: Seeing without eyes inside stirred vessels, Journal of Zhejiang University: Science, v 6 A, n 12, December, pp. 1379-1385, 2005.

Mann, R., Dickin, F.J., Wang, M., Dyakowski, T., Williams, R.A., Edwards, R.B., Forrest, A.E., Holden, P.J., Application of electrical resistance tomography to interrogate mixing processes at plant scale, Chem. Eng. Sci. 52 (13), pp. 2087-2097, 1997.

Mann, R., M, Wang, F.J. Dickin, T. Dyakowski,P.J. Holden. A.E. Forrest, and R.B. Edwards, Resistance tomography imaging of stirred vessel mixing at plant scale, Inst. Chem. Eng. Symo. Series, 140, pp. 155-166, 1996.

Metzner, A.B. and Taylor, J.S., Flow patterns in agitated vessels, AIChE J. 6, pp. 109-114 1960.

Moo-Young, M., K., Tichar and A.L. Takahashi, The blending efficiency of some impellers in batch mixing, AIChE J. 18, pp. 178-182, 1972.

Moreira, R.M., Pinto, A. F., Mesnier, R., Leclerc, J.-P. Influence of inlet positions on the flow behavior inside a photoreactor using radiotracers and coloured tracer investigations, Appli. Radi. Iso. 65 (4), pp. 419-427, 2007.

Nere, Nandkishor K., Ashwin W. Patwardhan, and Jyeshtharaj B. Joshi, Liquid-phase mixing in stirred vessels: turbulent flow regime, Ind. Eng. Chem. Res42, pp. 2661-2698, 2003.

Nienow, A. W., Lilly, M. D., Power drawn by multiple impellers in sparged agitated vessels. Biotechnol. Bioeng. 21, pp. 2341-2345. 1979.

Nishikawa, M., Ashiwake, K., Hashimoto, N., Nagata, S., Agitation power and mixing time in off-centring mixing. Int. Chem. Eng. 19 (1), pp. 153-159. 1979.

O'Connell F.D., and D.E. Mack, Simple turbines in fully baffled tanks, Chem. Eng. Prog. 46, pp. 358-362, 1950.

Ogawa, K., Ito, S., Matsumura, Y., Mixing rate in a stirred vessel. J. Chem. Eng. Japan. 13 (4), pp. 324-326, 1980.

Oppenländer, Thomas, Photochemical Purification of Water and Air, WILEY-VCH Verlag, GmhH &Co. KgaA,Weinheim, 2003.

Pinheiro, P.A. T., W.W. Loh, M. Wang, R.Mann, A.E. Forrest, and F.J. Dickin, Full three-dimensional electrical resistance tomography in a stirred vessel, Frontiers in Industrial Process Tomography, II, Delft, the Netherlands, pp. 251-256, 1997.

Plaskowski, A. (Andrzej), Imaging industrial flows: applications of electrical process tomography, Institute of Physics Pub., Bristol, UK. 1995.

Prousek, J., Advanced Oxidation Processes for water treatment photochemical processes, Chemicke Listy, 90 (5), pp. 307-315, 1996.

Raghav Rao, K. S. M. S., Design of multiphase reactors. Ph.D. Thesis, University of Bombay, Bombay, India, 1987.

Raghav Rao, K. S. M. S.; Joshi, J. B. Liquid phase mixing in mechanically agitated reactors. Chem. Eng. Commun. 74, pp. 1-25, 1988.

Rahimi, M., Mann, R., Macro-mixing, partial segregation and 3D selectivity fields inside a semi-batch stirred reactor. Chem. Eng. Sci., 56, pp. 763-771, 2001.

Ranade, V.V., J.R. Bourne, and J.B. Joshi, Fluid mechanics and blending in agitated tanks, Chem. Eng. Sci. 46, pp. 1883-1893, 1991.

Rewatkar, V. B., Joshi, J. B., Effect of impeller design on liquid phase mixing in mechanically agitated reactors. Chem. Eng. Commun. 102, pp. 1-34, 1991.

Rice, R.G., Applications of Ozone for industrial wastewater treatment-a review, Ozone Sci. Eng. 18, pp. 477-515, 1997.

Rielly, C.D. and R.E. Britter, Mixing times for passive tracers in stirred tanks, Proc. Of 5th European Conference on Mixing, Wurzburg, West Germany, pp. 365-375, 1985.

Rushton, J.H., Costich, E.W. and Everett H. J., Power characteristics of mixing impellers, Part 1, Chem. Eng. Progr. 46, pp. 395-402, (1950 a).

Rushton, J.H., Costich, E.W. and Everett H. J., Power characteristics of mixing impellers, Part 2, Chem. Eng. Progr. 46, pp. 467-476, (1950 b).

Sahle-Demessie, E., Bekele, S., Pillai, U.R., Residence time distribution of fluids in stirred annular photoreactor, Catalysis Today, 88 (1-2), pp. 61-72, 2003.

Sano, Y., Usui, H., Effects of paddle dimensions and baffle conditions on the interrelations among discharge flow rate, mixing power, and mixing time in mixing vessels. J. Chem. Eng. Jpn. 20 (4), pp. 399-404, 1987.

Scheible, O.K., Bassel, C.D., Ultroviolet disinfection in a secondary wastewater treatment plant effluent, EPA-600/S2-81-152, USEPA, 1981.

Scicchitano, T., Photoreactors: an overview, Ryerson University, CHE042 Thesis report, 2003.

Shang, C., Blatchley III E.R., Chlorination of pure bachterial cultures in aqueous solution, Wat. Res. 35, No. 1, pp. 244-254, 2001.

Shiue, S., and C.W. Wong, Studies on homogenization efficiency of various agitators in liquid blending, Can, J. Chem. Eng. 62, pp. 602-609, 1984.

Smith, J. M., Warmoeskerken, M. M. C. G., Zeef, E., Flow conditions in vessels dispersing gases in liquids with multiple impellers in biotechnology processes: scale-up and mixing; Ho, C. S., Oldshue, J. Y., Eds.; American Institute of Chemical Engineers: New York, pp. 107-115, 1987.

Snowball, M.R., Hornsey, I.S., Purification of water supplies using ultraviolet light, Developments in food microbiology, edited by Robinson RK. NY: Elsevier App. Sci., pp. 171-191, 1988.

Sörensen, M., Weckenmann, J., Galvanotechnik 89: 9, cited in: Sörensen, M., Weckenmann, J., XyanoMat ® - Moderne Cyanidentgiftung mittels UV-Oxidation, Anwendungsbeispiele aus der Praxis, a.c.k. aqua concept GmbH, Karlsruhe, Germany, 1988.

Sundstrom, D.W., Weir, B.A., Barber, T.A., Klei, H.E., Destruction of pollutants and microorganisms in water by UV light and hydrogen peroxide, Wat. Pollu. Res. J. Can., 27 (1), pp. 57-68, 1992.

Tabrizi, G.B., Meharvar, M., Piolo-plant study for the photochemical treatment of aquaeous linear alkylbenzene sulfonate, Sepa. Puri. Technol. 49, pp. 115-121, 2006.

Tapp, H.S., Peyton, A.J., Kemsley, E.K., Wilson, R.H., Chemical engineering applications of electrical process tomography, Sensors and Actuators, B: Chemical 92 (1-2), pp. 17-24, 2003.

Toye, D., Fransolet, E., Simon, D., Crine, M., L'Homme, G., Marchot, P., Possibilities and limits of application of electrical resistance tomography in hydrodynamics of bubble columns, Cana. J. Chem. Eng. 83(1), pp. 4-10, 2005.

Trageser, M., Greunig, H-J., Destruction of organic and inorganic complexes by UV-activated oxidation, procedding of the 2nd International Conference on Oxidation Technologies of Water and Wastewater Treatment, Clausthal-Zellerfeld, Germany, 28-31, May 2000, Wat. Sci. Technol. 44, issue 5; electronic release, 2000.

Ulrich, A., Wieser, J., Salvermoser, M., Murnich, D., Phys.Bl. 56 (6): 46-52; cited in: Zimmermann, R., 2002, On-line-prozess-und produktanalytic mit massenspektrometrie, Nachr. Chem. 50, pp. 166-169, 2000.

Vasconcelos, Jorge M. T., Sandra C. P. Orvalho, Ana M. A. F. Rodrigues, and Sebastião S. Alves, Effect of blade shape on the performance of six-bladed disk turbine impellers, Ind. Eng. Chem. Res. 39, pp. 203-213, 2000.

Voncken, R.M., D.B. Holmes and H.W. den Hartog, Fluid flow in turbine-stirred, baffled tanks-II, Dispersion during circulation, Chem, Eng. Sci. 19, pp. 209-213, 1964.

von Sonntag, C., The chemical basis of radiation biology , Taylor and Francis, London, 1987.

Vrábel, Peter., Rob G. J. M. van der Lans, Karel Ch. A. M. Luyben, Lotte Boon, Alvin W. Nienow, Mixing in large-scale vessels stirred with multiple radial or radial and axial up-pumping impellers: modelling and measurements, Chem. Eng. Sci. 55, pp. 5881-5896, 2000.

Wang, M. ; Dorward, A.; Vlaev, D.; Mann, R., Measurements of gas-liquid mixing in a stirred vessel using electrical resistance tomography (ERT), Chem. Eng. J., v 77, 1, pp. 93-98, 2000.

Wang, M., Yin, W., Measurements of the concentration and velocity distribution in miscible liquid mixing using electrical resistance tomography. Chem. Eng. Res. Des. 79(A8), pp. 883-886, 2001.

Ward, R.W., DeGrave GM. Residual toxicity of several disinfectants in domestic wastewater, JWPCF, pp. 50-46, 1978.

West, R.M., Jia, X., Williams, R.A., Parametric modelling in industrial process tomography, Chem. Eng. J. 77 (1-2), pp. 31-36, 2000.

Whitby, G.E., Scheible, O.K., The history of UV and wastewater, IUVA News; 6(3), pp. 15-26, 2004.

White SC, Jernigan EB., Venosa AD., A study of operational Ultraviolet disinfection equipment at secondary treatment plants, J.Wat. Poll. Contr. Fed. 58. No.3, pp. 181-192, 1986.

Williams RA, Beck MS., Process tomography: principles, techniques and applications. 7th ed. Oxford, UK: Butterworth-Heinemann, 1995.

Wolfe, R.L., Ultraviolet disinfection of potable water. Environ. Sci. Technol. 24 (6), pp. 768–773, 1990.

Wright, H.B., Sakamoto, G., UV dose required to achieve incremental log inactivation of bacteria, viruses, and protozoa. Trojan Tech Inc. revision of Sept. 12, 2001.

Xie, C.G., Reinecke, N., Beck, M.S., Mewes, D., Williams, R.A., Electrical tomography techniques for process engineering applications, Chem. Eng. J. Bioche. Eng. J. 56 (3), pp. 127-133,1995.

XMa, A J Peyton, S R Higson, A Lyons and S J Dickinson, Hardware and software design for an electromagnetic induction tomography (EMT) system for high contrast metal process applications, Meas. Sci. Technol. 17, pp. 111–118, 2006.

Yin, X., Xin, F., Zhang, F., Wang, S., Zhang, G., Kinetic study on photocatalytic degradation of 4BS Azo dye over TiO_2 in slurry, Environ. Eng. Sci. 23 (6), pp. 1000-1008, 2006.

York, T.A., Davidson, J.L., Mazurkiewich, L., Mann, R., Grieve, B.D., Towards process tomography for monitoring pressure filtration, IEEE Sensors Journal 5 (2), pp. 139-151, 2005.

Yorkey T.J., Webster J.G. and Tompkins W.J., An optimal impedance tomographic reconstruction algorithm, Proc. Annu. Int. Conf. IEEE En g. Med Biol. Soc., 8, pp. 339-342, 1986.

Yue, P.L., Legrini, O., Photochemical degradation of organics in water, Wat. Pollu. Res. J. of Can., 27 (1), pp. 123-137, 1992.

Yuen, E.L., Mann, R., York, T.A., Grieve, B.D., Electrical resistance tomography (ERT) imaging of a metal-walled solid–liquid filter, in: Proceedings of the Second World Congress on Industrial Process Tomography, Hannover, Germany, 29–31 August pp. 183–190, 2001.

APPENDIX

EXPERIMENTAL DATA TABLES

Table A.1 Dynamic data (impeller RT6, $\mu = 1.00\times10^{-3}$ Pa·s, $V = 5.34\times10^{-2}m^3$)

Speed, N (rpm)	Mixing Torque, τ (m·N)	Power, P (W)	N_p	Re	P_m (Watt/kg)	$N^3D^5\times 10^{-4}/V$
24	0.004	0.01	4.21	6546.36	0.0002	0.41
45	0.009	0.04	2.83	12263.47	0.0008	2.72
53	0.011	0.06	2.50	14443.65	0.0011	4.44
68	0.024	0.17	3.41	18531.47	0.0032	9.37
85	0.047	0.41	4.24	23164.34	0.0078	18.31
101	0.070	0.74	4.51	27524.68	0.0138	30.71
118	0.093	1.15	4.39	32157.55	0.0215	48.98
142	0.134	1.99	4.36	38698.07	0.0372	85.35
167	0.184	3.22	4.35	45511.11	0.0604	138.83
193	0.235	4.75	4.16	52596.67	0.0891	214.29
202	0.262	5.55	4.23	55049.37	0.1039	245.69
234	0.342	8.38	4.11	63770.06	0.1571	381.93
258	0.425	11.48	4.20	70310.58	0.2152	511.91
295	0.565	17.46	4.28	80393.88	0.3272	765.24
331	0.717	24.84	4.31	90204.66	0.4654	1080.97
386	0.976	39.44	4.31	105193.35	0.7390	1714.32
422	1.180	52.14	4.36	115004.13	0.9770	2240.10
463	1.424	69.07	4.37	126177.51	1.2942	2958.52
569	2.177	129.73	4.43	155064.80	2.4310	5491.21
586	2.307	141.57	4.42	159697.67	2.6528	5998.24
644	2.798	188.68	4.44	175503.93	3.5356	7961.38
712	3.442	256.66	4.47	194035.40	4.8094	10758.98
728	3.604	274.75	4.48	198395.74	5.1484	11500.72
773	4.080	330.24	4.49	210659.21	6.1882	13767.95

Table A.2 Dynamic data (impeller PBTU, $\mu = 1.00\times10^{-3}$ Pa·s, $V = 5.34\times10^{-2}m^3$)

Speed, N (rpm)	Mixing Torque, τ (m·N)	Power, P (W)	N_p	Re	P_m (Watt/kg)	$N^3D^5\times 10^{-4}/V$
35	0.004	0.01	1.91	9616.29	0.0002	0.65
39	0.004	0.02	1.69	10781.88	0.0003	1.39
46	0.005	0.02	1.56	12535.99	0.0005	2.90
56	0.006	0.04	1.28	15440.92	0.0007	5.52
80	0.018	0.15	1.89	21801.73	0.0029	15.26
110	0.03	0.35	1.64	29977.38	0.0065	39.67
146	0.055	0.84	1.7	39788.16	0.0158	92.77
172	0.07	1.27	1.57	46873.72	0.0238	151.68
191	0.086	1.72	1.56	52051.63	0.0323	207.70
214	0.11	2.46	1.58	58319.63	0.0461	292.13
256	0.157	4.2	1.57	69765.54	0.0786	500.09
300	0.214	6.73	1.57	81756.49	0.1261	804.81
360	0.3	11.32	1.52	98107.78	0.2121	1390.72
400	0.363	15.19	1.49	109008.65	0.2846	1907.70
476	0.515	25.67	1.5	129720.29	0.481	3214.78
508	0.579	30.82	1.48	138440.98	0.5775	3907.71
570	0.726	43.36	1.47	155337.33	0.8125	5520.21
620	0.877	56.91	1.5	168963.41	1.0664	7104.05
645	0.947	63.99	1.5	175776.45	1.1991	7998.53
680	1.04	74.03	1.48	185314.7	1.3872	9372.55
732	1.196	91.65	1.47	199485.83	1.8024	11691.34
767	1.34	107.63	1.5	209024.09	2.0168	13449.84

Table A.3 Dynamic data (impeller RT6, N = 45 rpm, C = 13 cm)

Radial distance, r (cm)	Angle, θ (deg)	Mixing time, t_{95} (s)
10	0	47
10	15	46
10	30	44
10	45	42
11.5	0	53
11.5	15	47
11.5	30	42
11.5	45	40
13	0	65
13	15	51
13	30	47
13	45	44
14.5	15	50
14.5	30	48
14.5	45	45
16	15	59
16	30	46
16	45	39

Table A.4 Dynamic data (impeller RT6, N = 150 rpm, C = 13 cm)

Radial distance, r (cm)	Angle, θ (deg)	Mixing time, t_{95} (s)
10	0	28
10	15	26
10	30	24
10	45	22
11.5	0	20
11.5	15	19
11.5	30	16
11.5	45	14
13	0	30
13	15	26
13	30	25
13	45	20
14.5	15	23
14.5	30	15
14.5	45	14
16	15	17
16	30	14
16	45	12

Table A.5 Dynamic data (impeller RT6, N = 250 rpm, C = 13 cm)

Radial distance, r (cm)	Angle, θ (deg)	Mixing time, t_{95} (s)
10	0	18
10	15	16
10	30	16
10	45	16
11.5	0	18
11.5	15	16
11.5	30	16
11.5	45	16
13	0	21
13	15	19
13	30	19
13	45	19
14.5	15	17
14.5	30	17
14.5	45	17
16	15	15
16	30	15
16	45	15

Table A. 6 Dynamic data (impeller RT6, N = 350 rpm, C = 13 cm)

Radial distance, r (cm)	Angle, θ (deg)	Mixing time, t_{95} (s)
10	0	-
10	15	-
10	30	-
10	45	-
11.5	0	15
11.5	15	13
11.5	30	13
11.5	45	13
13	0	17
13	15	15
13	30	15
13	45	13
14.5	15	13
14.5	30	13
14.5	45	13
16	15	13
16	30	13
16	45	13

Table A.7 Dynamic data (impeller RT6, N = 500 rpm, C = 13 cm)

Radial distance, r (cm)	Angle, θ (deg)	Mixing time, t_{95} (s)
10	0	-
10	15	-
10	30	-
10	45	-
11.5	0	12
11.5	15	9
11.5	30	9
11.5	45	9
13	0	15
13	15	10
13	30	10
13	45	10
14.5	15	9
14.5	30	9
14.5	45	9
16	15	9
16	30	9
16	45	9

Table A.8 Dynamic data (impeller PBTU, N = 45 rpm, C = 13 cm)

Radial distance, r (cm)	Angle, θ (deg)	Mixing time, t_{95} (s)
10	0	55
10	15	51
10	30	49
10	45	46
11.5	0	56
11.5	15	54
11.5	30	52
11.5	45	50
13	0	61
13	15	58
13	30	54
13	45	51
14.5	15	56
14.5	30	54
14.5	45	47
16	15	49
16	30	48
16	45	46

Table A.9 Dynamic data (impeller PBTU, N = 250 rpm, C = 13 cm)

Radial distance, r (cm)	Angle, θ (deg)	Mixing time, t_{95} (s)
10	0	13
10	15	12
10	30	12
10	45	12
11.5	0	14
11.5	15	13
11.5	30	13
11.5	45	13
13	0	14
13	15	13
13	30	13
13	45	13
14.5	15	12
14.5	30	12
14.5	45	12
16	15	12
16	30	12
16	45	12

Table A.10 Dynamic data (impeller RT6, N = 45 rpm, C = 23.4 cm)

Radial distance, r (cm)	Angle, θ (deg)	Mixing time, t_{95} (s)	Average mixing time (s)	Standard deviation, σ
r=10 cm	0	59	58.5	0.71
		58		
	15	57	57	0.00
		57		
	30	54	54	0.00
		54		
	45	51	52	1.41
		53		
r=11.5 cm	0	59	59	0.00
		59		
	15	55	55.5	0.71
		56		
	30	50	51	1.41
		52		
	45	49	49.5	0.71
		50		
r=13 cm	0	60	60	0.00
		60		
	15	52	52	0.00
		52		
	30	48	48	0.00
		48		
	45	44	45.5	2.12
		47		
r=14.5 cm	15	57	56.5	0.71
		56		
	30	53	53.5	0.71
		54		
	45	43	43.5	0.71
		44		
r=16 cm	15	54	54.5	0.71
		55		
	30	52	52.5	0.71
		53		
	45	52	50.5	2.12
		49		

Table A.11 Dynamic data (impeller RT6, N = 250 rpm, C = 23.4 cm)

Radial distance, r (cm)	Angle, θ (deg)	Mixing time, t_{95} (s)	Average mixing time (s)	Standard deviation, σ
r=10 cm	0	14	14.5	0.71
		15		
	15	12	12	0.00
		12		
	30	12	12.5	0.71
		13		
	45	11	11.5	0.71
		12		
r=11.5 cm	0	15	15	0.00
		15		
	15	12	12	0.00
		12		
	30	11	11.5	0.71
		12		
	45	12	11.5	0.71
		11		
r=13 cm	0	18	18.5	0.71
		19		
	15	10	11	1.41
		12		
	30	12	11.5	0.71
		11		
	45	11	11	0.00
		11		
r=14.5 cm	15	12	12	0.00
		12		
	30	13	12.5	0.71
		12		
	45	12	12	0.00
		12		
r=16 cm	15	13	13	0.00
		13		
	30	13	13	0.00
		13		
	45	11	11	0.00
		11		

Table A.12 Dynamic data (impeller RT6, C =13 cm)

Speed, N (rpm)	Mixing Torque, τ (m·N)	Power, P (W)	P_m (Watt/kg)	UV tubes locations	Mixing time, t_{95} (s)
45	0.01	0.04	0.001	A	39
				B	65
				C	42
250	0.58	30.37	0.569	A	15
				B	21
				C	16
350	0.27	9.98	0.187	A	13
				B	17
				C	13
500	0.16	4.14	0.078	A	9
				B	15
				C	10

Location A: r =16cm, $\theta = 45^{o}$;

Location B: r =13 cm, $\theta = 0^{o}$;

Location R: r =11.5 cm, $\theta = 30^{o}$.

Table A.13 Dynamic data (impeller PBTU, C = 13 cm)

Speed, N (rpm)	Mixing Torque, τ (m·N)	Power, P (W)	P_m (Watt/kg)	UV tubes locations	Mixing time, t_{95} (s)
45	0.01	0.04	0.001	A	37
				B	61
				C	40
250	0.40	10.43	0.195	A	13
				B	14
				C	13
350	0.80	29.41	0.551	A	9
				B	13
				C	11
500	1.66	86.92	1.629	A	7
				B	9
				C	7

Location A: r =16cm, $\theta = 45^{o}$;

Location B: r =13 cm, $\theta = 0^{o}$;

Location R: r =11.5 cm, $\theta = 30^{o}$.

Table A.14 Dynamic data (impeller RT6, UV tubes location: A)

Clearance, C (cm)	Speed, N (rpm)	Mixing Torque, τ (m·N)	Power, P (W)	P_m (Watt/kg)	Mixing time, t_{95} (s)
13 cm	100	0.07	0.73	0.014	20
	200	0.26	5.45	0.102	16
	300	0.58	18.22	0.341	12
	400	1.08	45.24	0.848	8
21.45 cm	100	0.07	0.73	0.014	23
	200	0.26	5.45	0.102	17
	300	0.58	18.22	0.341	14
	400	1.08	45.24	0.848	12
29.9 cm	100	0.07	0.73	0.014	37
	200	0.26	5.45	0.102	21
	300	0.58	18.22	0.341	15
	400	1.08	45.24	0.848	13
38.35 cm	100	0.07	0.73	0.014	44
	200	0.26	5.45	0.102	23
	300	0.58	18.22	0.341	16
	400	1.08	45.24	0.848	14

Table A.15 Dynamic data (impeller PBTU, UV tubes location: A)

Clearance, C (cm)	Speed, N (rpm)	Mixing Torque, τ (m·N)	Power, P (W)	P_m (Watt/kg)	Mixing time, t_{95} (s)
13 cm	100	0.03	0.28	0.005	19
	200	0.10	2.05	0.038	15
	300	0.21	6.60	0.124	11
	400	0.36	15.08	0.283	7
21.45 cm	100	0.03	0.28	0.005	22
	200	0.10	2.05	0.038	16
	300	0.21	6.60	0.124	13
	400	0.36	15.08	0.283	10
29.9 cm	100	0.03	0.28	0.005	28
	200	0.10	2.05	0.038	19
	300	0.21	6.60	0.124	15
	400	0.36	15.08	0.283	12
38.35 cm	100	0.03	0.28	0.005	29
	200	0.10	2.05	0.038	20
	300	0.21	6.60	0.124	16
	400	0.36	15.08	0.283	13